energies

Review

Power Converter Topologies for Grid-Tied Solar Photovoltaic (PV) Powered Electric Vehicles (EVs)—A Comprehensive Review

Fatemeh Nasr Esfahani [1], Ahmed Darwish [1] and Barry W. Williams [2,*]

[1] School of Engineering, Lancaster University, Lancaster LA1 4WY, UK; f.nasresfahani@lancaster.ac.uk (F.N.E.); a.badawy@lancaster.ac.uk (A.D.)
[2] Department of Electronic and Electrical Engineering, University of Strathclyde, Glasgow G1 1XQ, UK
* Correspondence: barry.williams@strath.ac.uk

Abstract: The transport sector generates a considerable amount of greenhouse gas (GHG) emissions worldwide, especially road transport, which accounts for 95% of the total GHGs. It is commonly known that Electric vehicles (EVs) can significantly reduce GHG emissions. However, with a fossil-fuel-based power generation system, EVs can produce more GHGs and therefore cannot be regarded as purely environmentally friendly. As a result, renewable energy sources (RES) such as photovoltaic (PV) can be integrated into the EV charging infrastructure to improve the sustainability of the transportation system. This paper reviews the state-of-the-art literature on power electronics converter systems, which interface with the utility grid, PV systems, and EVs. Comparisons are made in terms of their topologies, isolation, power and voltage ranges, efficiency, and bi-directional power capability for V2G operation. Specific attention is devoted to bidirectional isolated and non-isolated EV-interfaced converters in non-integrated architectures. A brief description of EV charger types, their power levels, and standards is provided. It is anticipated that the studies and comparisons in this paper would be advantageous as an all-in-one source of information for researchers seeking information related to EV charging infrastructures.

Keywords: photovoltaic systems (PV); electric vehicles (EVs); PV grid-connected; PV stand-alone; vehicle-to-grid (V2G); integrated topologies; non-integrated topologies; isolation; grid integration

Citation: Nasr Esfahani, F.; Darwish, A.; Williams, B.W. Power Converter Topologies for Grid-Tied Solar Photovoltaic (PV) Powered Electric Vehicles (EVs)—A Comprehensive Review. *Energies* **2022**, *15*, 4648. https://doi.org/10.3390/en15134648

Academic Editor: Enrique Romero-Cadaval

Received: 1 June 2022
Accepted: 22 June 2022
Published: 24 June 2022

1. Introduction

According to the World Health Organization (WHO), air pollution has been responsible for almost 18% of premature births and over 3.7 million death tragedies worldwide [1]. As the biggest contributor, internal combustion engine (ICE) vehicles burning fossil fuels (e.g., gasoline, diesel, etc.) are responsible for 29% of the total GHG emissions in the USA [2]. Growing public concerns about environmental problems and rising demand for fossil fuels have been major factors in accelerating the growth of environmentally friendly and zero-emission means of transportation, specifically electric vehicles (EVs), including hybrid electric vehicles (HEVs), battery electric vehicles (BEVs), and plug-in electric vehicles (PEVs) [3]. Despite the COVID-19 pandemic, the total number of EV sales experienced a 43% increase from 2019 to 2020 [4]. The projected growth of EV sales from 3.1 million in 2020 to 14 million in 2025 calls for a corresponding development in the charging facilities [2]. The high cost of batteries and their short lifespan, EV reliability issues, limited driving range, and charging time are all key barriers to accepting EVs as an alternative for IEC vehicles [5,6].

Furthermore, the large-scale penetration of EVs may impose strain on the grid during charging periods as they demand a huge amount of electrical energy in a short time. Because the present utility grid in many countries is predominantly powered by a fossil fuel-based generation system, EVs cannot be deemed completely eco-friendly [7].

Integrating Renewable Energy Sources (RESs) including wind, biomass, and solar into EV charging infrastructures is gaining popularity as they can reduce the burden on the electricity grid, charging costs, and GHG emissions [8,9]. Wind energy has attracted much attention due to its low cost, sustainability, and rapid growth. Furthermore, it can be constructed on current farms, bringing additional income to owners [10]. It has been reported by the Global Wind Energy Council (GWEC) that renewable energy will deliver 25% of the global electricity demand in 2035 wherein wind energy will account for a quarter [11]. Biomass-based electricity production from waste streams such as Municipal Solid Wastes (MSW), animal wastes, and food processing wastes also offers many advantages, of sustainability, such as carbon neutrality, domestic production, versatility, availability, efficiently managing waste produced, and not being subjected to price fluctuations [12,13]. In 2020, bioenergy electricity generation increased by 53 TWh (+8%) when compared with 2019, which exceeds the 7% annual rate needed through 2030 in the Net Zero Emissions by 2050 Scenario [14]. Solar power is an environmentally friendly energy source [15]. Low-carbon PV power generation is attracting substantial interest owing to a significant reduction in installation costs over recent decades [3,8]. Improvements in efficiency and a continuous drop in the price of materials utilised (e.g., crystalline silicon (c-Si), amorphous silicon (a-Si), gallium arsenide (GaAs), organometallics (soluble platinum), etc.) have all contributed to the total cost reduction [16]. Furthermore, a PV system requires minimal maintenance [8]. Therefore, it has been preferred over other RESs for EV charging. There are several benefits to PV solar-powered EV charging, such as (i) reduced grid power demand, (ii) installation feasibility, (iii) free of emissions, (iv) lower fuel cost, and (v) significant cost savings, as the charging occurs during the peak demand period with high tariffs [1,17,18]. Additionally, the EV battery can function as an energy storage unit (ESU) to store PV energy when required, alleviating problems associated with large-scale PV integration into the electricity grid.

Exiting EV chargers are generally categorised into three levels. Level-1 chargers have the lowest ratings, where the peak power is approximately 3.75 kW. In Level 2, the peak power can reach 22 kW, and therefore, they are becoming more popular as they reduce the charging time considerably. Three-phase Level-3 AC chargers can provide a power rating greater than 14.4 kW and up to 43.5 kW (e.g., Renault Zoe). Usually, IEC 60,309 and IEC 62198-2 connectors are used in these chargers. Level-3 DC chargers can provide 350 kW of power directly to the battery [1]. SAE J1772, CHAdeMO, and IEC 62,196 are the main standards for Level-3 DC chargers. Unlike Level-1 chargers where the converter can be installed within the car (on-board battery chargers), the converters employed in Level-2 and Level-3 AC chargers are bulkier and heavier, so the charger is not located within the car (off-board battery chargers) [1,2].

There are two ways to use PV panels for charging EVs, namely PV-grid (on-grid) and PV-standalone (off-grid) [8,19]. PV-standalone refers to charging an electric vehicle solely with solar energy without involving the grid. Because PV power is inherently variable, a connection to the electricity grid is required to ensure a consistent secure supply of electricity for EV charging. The PV array, a DC–DC converter equipped with maximum power point tracking (MPPT), and a DC–DC converter at the EV port, are common hardware components in PV-standalone and PV-grid charging systems [8], while another power stage (AC–DC) is required in an on-grid EV charging system. If both the EV-interfaced and grid-interfaced converters can support bidirectional power flow, vehicle-to-grid (V2G) can be implemented to increase grid stability during peak load hours [20]. To meet international safety standards (e.g., IEC 62955, IEC 61851) [21–23], solar PV and the electricity grid are required to be isolated from the EV batteries [24]. The isolation can be implemented using either a high-frequency (HF) transformer in the kHz range associated with the EV-interfaced converter or a grid-connected low-frequency (LF) transformer.

Power electronic converters play a crucial role in EV charging systems to deliver the highest possible power at high efficiency. Converter topologies employed in the PV-grid charging stations can be classified as non-integrated and integrated architectures [17,18,25]. There are three converters dominating the non-integrated architectures, namely the PV-interfaced converter [3,26], the grid-interfaced converter [27–54], and the EV-interfaced converter [55–85]. For efficient charging, each converter requires a specific controller, which adds to the complexity and increases the total power losses. Alternatively, a single integrated converter comprised of sub-converters interfacing with the EV, PV, and grid can be used [18,86–89]. Although extra switches are required for integration, the entire integrated system has a reduced number of devices when compared with its non-integrated counterpart.

Reviews of power electronics converter architectures for DC fast chargers have been presented in [2,26]. However, they lack information about how the EV battery chargers are supplied by both PV solar power and the local AC grid. In addition, the studies on the PV-EV-grid charging architecture in [3,8,9] have not covered all the potential PV, EV, and grid-interfaced converter topologies, particularly those proposed in recent publications. Therefore, it appears that there is an absence of an updated and thorough overview of these topics. In this paper, power converter topologies for PV-grid and PV-stand-alone charging infrastructures are comprehensively reviewed. Specific attention is devoted to bidirectional isolated and non-isolated EV-interfaced converters, which play a fundamental role in delivering power to EV batteries. For a broader readership, this work contains a concise explanation of EV battery charging types and their relevant standards.

The following outline is provided to facilitate reader navigation through the paper. The Global PV system deployment is presented in Section 2. EV charger types, power levels, and their standards are briefly described in Section 3. PV-grid and PV stand-alone EV charging structures are provided in Section 4. PV-interfaced, grid-interfaced, and EV-interfaced converters for non-integrated architectures are comprehensively reviewed and compared in the first subsection of Section 5, while the second subsection deals with multi-port integrated topologies and associated sub-converters. After giving some direction for the future research in Section 6, concluding remarks are drawn in Section 7.

2. International Deployment of Solar Photovoltaic (SPV) Systems

Solar PV power accounts for 3.1% of all electricity worldwide. Even the COVID-19 pandemic did not significantly impact solar deployment in 2020, given that installed renewable power capacity increased by more than 256 gigawatts (GW) during the pandemic, the highest increase ever [90]. Global PV capacity increased from 17 GW_{DC} to 139 GW_{DC} between 2010 and 2020 (see Figure 1). European markets led at the start of the decade, but PV growth shifted to Asia. By 2020, 57% of cumulative PV installations were in Asia, 22% in Europe, and 15% in the USA. At the end of the last decade, Germany, China, Japan, the USA, and India led the dominant markets in terms of cumulative PV installations. In 2020, China's yearly PV installations increased by 60%, accounting for more than one-third of global deployment. In terms of both cumulative and annual installations, the USA was the second-largest PV market. PV installations climbed dramatically in many important markets, including the USA, within the first nine months of 2021. India installed 177% more solar panels than it did in the same period in 2020 during the same period in 2021. In total, 171 GW of PV was added worldwide by the end of 2021. As predicted by analysts, annual global PV installations will continue to rise, with an average projection of 209 GW_{DC} and 231 GW_{DC} in 2022 and 2023, respectively [1,91].

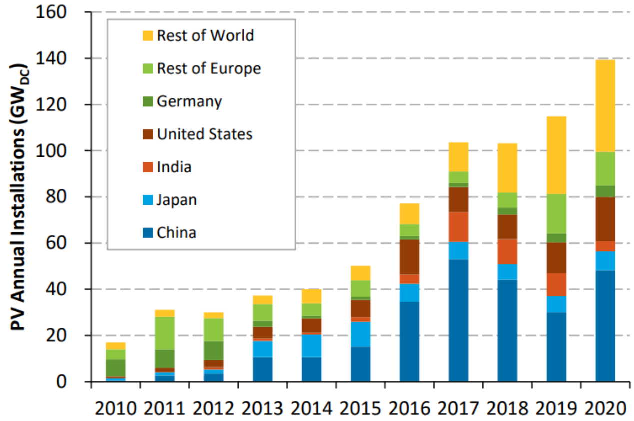

Figure 1. PV annual installations from 2010 to 2020 [90,91].

3. EVs Charger Types and Relevant Standards

In general, an EV (e.g., train, truck/bus, motorcycles/scooters, and electric cars) is powered by at least one electric motor and uses at least one battery as an energy storage system. The term "electric vehicle" in this paper alludes to battery electric vehicles (BEVs), hybrid electric vehicles (HEVs), and plug-in electric vehicles (PEVs) [2]. Large-scale acceptance of EVs into the vehicle market, which is currently dominated by the Ford Fusion, Toyota Prius, Honda, Chevrolet Volt, Nissan Leaf, Tesla, and BMW, is reliant on the successful and extensive implementation of the EV charging stations infrastructure [24]. Battery chargers for EVs can either be implemented externally (off-board) or inside the vehicle (on-board), as shown in Figure 2. The benefits and critical challenges for both on-board and off-board chargers are listed in Table 1.

Nowadays, most EVs have off-board DC fast chargers in addition to an on-board charger (OBC) embedded [illegible] V, which is used for slow charging overnight [illegible] mary is[illegible]lated to an OBC is the vo[illegible] 120 Vac), and hence charging power li[illegible]ions caused by space and [illegible]ht issu[illegible]dition to cost constraints. Nevertheless, as EV battery capacity grow[illegible] pow[illegible]Cs drastically increases. Early EVs using OBCs could only charge at 3.3 kW, but almost all EVs can now charge at 6.6 kW, 7.4 kW, 11 kW, and more (up to 20 kW) [92,93]. Despite the higher cost of off-board DC [illegible]ging s[illegible] they offer s[illegible]ive [illegible] lightening the EV's wei[illegible]nd cha[illegible] much highe[illegible]vel[illegible]er [illegible]) compared to their on-board counterparts.

The charging power level is usu[illegible]-off between charging time and EV charging infrastructure cost. Th[illegible]o methods of charging: AC and DC. AC cha[illegible]th Level-1, Level-2, and Level-3 charging delivers an AC supply, which is then converted into DC to charge the batteries through OBCs [9,93].

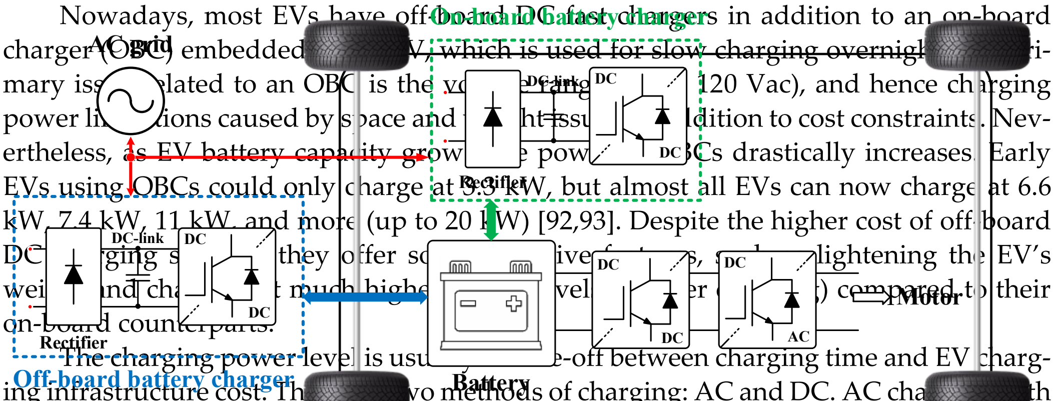

Figure 2. EV charging systems, including on-board and off-board chargers.

Table 1. Comparison between on-board and off-board battery chargers.

Charger	Size	Weight	Charging Duration	Power Range	Benefits	Challenges
Off-board	Medium/Large	Heavy	Short	Up to 400 kW	• Charge at higher power levels • Removed weight on EV • Fast charging	• Battery heating issues • Inflexible to charge at various places • More complex and higher cost
On-board	Small	Light	Long	Less than 50 kW	• Flexible to charge at various places • Cutting down on the amount of equipment needed by end-user • Less complex and lower cost	• Charge at lower power levels • Slow charging • Added EV weight

Level-1 AC charging offers the lowest power and is commonly installed in residential complexes for overnight charging. It takes 120 Vac/230 Vac as the input voltage and provides approximately 1.92 kW output power. Level-2 AC charging takes an input voltage of 208 Vac or 240 Vac and delivers up to 20 kW of power. Level-3 AC chargers (400 Vac

Table 1. *Cont.*

Charger	Size	Weight	Charging Duration	Power Range	Benefits	Challenges
On-board	Small	Light	Long	Less than 50 kW	• Flexible to charge at various places • Cutting down on the amount of equipment needed by end-user • Less complex and lower cost	• Charge at lower power levels • Slow charging • Added EV weight

Nowadays, most EVs have off-board DC fast chargers in addition to an on-board charger (OBC) embedded in the EV, which is used for slow charging overnight. The primary issue related to an OBC is the voltage range (up to 120 Vac), and hence charging power limitations caused by space and weight issues, in addition to cost constraints. Nevertheless, as EV battery capacity grows, the power in OBCs drastically increases. Early EVs using OBCs could only charge at 3.3 kW, but almost all EVs can now charge at 6.6 kW, 7.4 kW, 11 kW, and more (up to 20 kW) [92,93]. Despite the higher cost of off-board DC charging stations, they offer some attractive features, such as lightening the EV's weight and charging at much higher power levels (quicker charging) compared to their on-board counterparts.

The charging power level is usually a trade-off between charging time and EV charging infrastructure cost. There are two methods of charging: AC and DC. AC charging with Level-1, Level-2, and Level-3 charging delivers an AC supply, which is then converted into DC to charge the batteries through OBCs [9,93].

Level-1 AC charging offers the lowest power and is commonly installed in residential complexes for overnight charging. It takes 120 Vac/230 Vac as the input voltage and provides approximately 1.92 kW output power. Level-2 AC charging takes an input voltage of 208 Vac or 240 Vac and delivers up to 20 kW of power. Level-3 AC chargers (400 Vac, three-phase, 32–63 A) have a power rating higher than 14.4 kW and up to 43.5 kW. They recharge the EV battery pack in no more than two hours [1]. Level-3 DC fast chargers (off-board), which can handle power between 50 kW and 300 kW, have grown in popularity due to the limited power rating and longer charging time of on-board Level-1, Level-2, and Level-3 AC chargers. Level-3 DC fast chargers can deliver DC voltage of 300 V or more, up to 800 V, and charge existing EV batteries in under 30 min. DC chargers are positioned off-board due to high power flow, allowing the vehicle's weight and capacity to be minimised. DC charging (off-board chargers), however, necessitates more complex infrastructures as the output voltage must be adapted to various EVs encountered at the charging stations.

Table 2 lists the charging levels, specifications, and standards for electric vehicles. In terms of standardisation, three central global organisations rival each other to be the de facto standard for EV charging: (i) CHAdeMO association, (ii) the Society of Automotive Engineering (SAE), and (iii) the International Electro-technical Commission (IEC). Besides, Tesla Motors has proposed an exclusive set of EV charging standards [9,19]. In the United States, the Level-2 AC charging connector is a proprietary Tesla plug or the SAEJ1772 Type-1, whereas, in Europe, the IEC62196-2 Type-2 plug is used [22,94,95]. IEC 60309, IEC 62198-2-Mennekes, and 62198-2-Same connectors are generally used in EV chargers at level-3 AC chargers [1].

Table 2. EVs charging levels, specifications, and standards.

Charging Station Type	On-Board/Off-Board	Supply	Single/Three Phase	Power Range (kW)	Charging Time	Battery Capacity (kWh)	Charging Location	Protection Type	Standards
Level-1 (AC)	On-board	120/230 Vac 12–16 A	Single	1.44–1.92	11–36 h	16–50	Residential	Breaker in cable	SAE J1772
Level-2 (AC)	On-board	208/240 Vac 15–80 A	Single/split phase	3.1–19.2	2–6 h	16–30	Home or workplace	Pilot function and breaker in cable	SAE J1772 IEC 62196 IEC 60309 IEC 62198
Level-3 (AC)	On-board	400 Vac 32–63 A	Three phase	14.4–43.5	<2 h	~15	Home or workplace	Pilot function and breaker in cable	SAE J1772 IEC 60309 IEC 62198
Level-3 (DC)	Off-board	300–600 Vdc Up to 400 A	Three phase	>400	<30 min	20–50	Public (like gas stations)	Monitoring and communication between EV and charging station	SAE J1772 IEC 62196 CHAdeMO Tesla

4. PV-Grid and Stand-Alone EV Charging

The rapid growth in EV numbers has brought a new issue: An additional burden on the electricity grid caused by the extremely high current drawn for EV fast charging, particularly during rush hour when electricity tariffs and load demand are at their highest [96,97]. Building renewable energy source (RES)-based EV charging stations is one viable solution. With a steady rise in PV annual installations (see Figure 1) and a downward trend in PV module prices, solar power is becoming more widely recognised as a cost-effective source of energy to complement the electricity grid, and the integration of PV into EV charging systems is becoming more common [98,99].

PV-grid (on-grid) and PV-standalone (off-grid) are two possible options for charging an EV with solar power, and their block diagrams are shown in Figure 3a,b, respectively. PV stand-alone EV charging, which stands for charging an EV only through PV power and without utilising the utility grid, is more advantageous in rural or depopulated locations where utility supply is unavailable, limited, or relatively expensive [100,101]. The PV array, on the other hand, should be reasonably large to meet the charging requirements for a large number of EVs [102]. Furthermore, because of the intermittent nature of PV power, a grid connection is required to ensure a consistent supply of electricity for EV charging. In other words, EV charging could be continuously conducted through a PV-grid EV charging system since the charger can switch to the utility grid when there is inadequate solar irradiation or variations in ambient conditions (e.g., temperature). It is also flexible because solar PV power can be injected into the electricity grid in the absence of EVs. From a practical standpoint, the main distinction between the on-grid and off-grid architectures is the bidirectional grid-interfaced power converter (which can act as both an inverter and a rectifier). PV arrays, DC–DC converters with built-in MPPT, and bidirectional DC converters for charging and discharging batteries are all common hardware components in on- and off-grid charging systems [1].

In a PV stand-alone architecture, the charging system must include an ESU, which allows extra energy to be stored. This energy then can later be used to charge the EV when the PV power is unavailable (e.g., overnight). The ESU can also be utilised in a PV-grid charging system to lessen the negative impact of EV charging on the electricity grid [103]. However, with ESU integration, one power stage is added, leading to increased controller complexity and battery charger implementation costs. Despite the fact that the off-grid charging system appears to be considerably simpler and more efficient thanks to the fewer power conversion stages involved, the PV-grid system has proven to be more profitable and currently preferred [1].

PV-grid charging systems can typically operate in 10 different modes based on the interaction among the PV array, EVs, the grid, and the ESU. The charging station operation in a PV-grid charging system can be adjusted such that it is supplied by the utility grid, of EVs [102]. Furthermore, because of the intermittent nature of PV power, a grid connection is required to ensure a consistent supply of electricity for EV charging. In other words, EV charging could be continuously conducted through a PV-grid EV charging system since the charger can switch to the utility grid when there is inadequate solar irradiation or variations in ambient conditions (e.g., temperature). It is also flexible because solar PV power can be injected into the electricity grid in the absence of EVs. From a practical standpoint, the main distinction between the on-grid and off-grid architectures is the bidirectional grid-interfaced power converter (which can act as both an inverter and a rectifier). PV arrays, DC–DC converters with built-in MPPT, and bidirectional DC–DC converters for charging and discharging batteries are all common to both on- and off-grid charging systems [1].

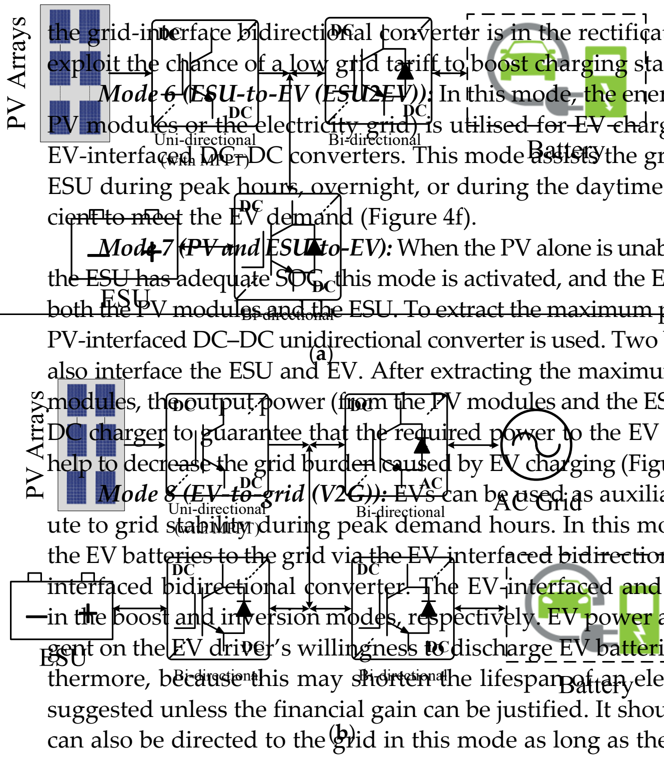

Figure 3. EV charging systems: (**a**) PV standalone (off-grid) and (**b**) PV-grid (on-grid).

power conversion stages involved, the PV-grid system has proven to be more profitable and currently preferred [1].

PV-grid charging systems can typically operate in different modes depending on the interaction among the PV array, EVs, the grid, and ESU. The charging station operation in a PV-grid charging system can be adjusted such that it is supplied by the utility grid, PV power, or both. Furthermore, vehicle-to-grid (V2G) technology can be implemented to improve grid stability during peak hours [26].

Mode 1 (PV-to-EV (PV2EV)): If the PV energy is adequate to charge the EV, the PV will handle the full charging process, and grid power is not used in the EV charging process. As shown in Figure 4a, the PV-interfaced DC–DC converter and the DC charger at the EV side are used for this purpose. When the EV's state-of-charge (SOC) reaches its maximum, EV charging stops, and the surplus power generated by the PV arrays will be fed into the grid via the grid-interfaced DC–AC converter.

Mode 2 (grid-to-EV (G2EV)): The EV can be charged from the electricity grid alone if the PV system is completely incapable of generating any power due to unfavourable weather conditions, during the night, or when the PV system is in a fault situation. The grid-interfaced bidirectional converter is in the rectification mode, converting grid AC power to DC. The EV-interfaced DC–DC converter is used to adjust the DC voltage (Figure 4b).

Mode 3 (PV and grid-to-EV): If available PV power is inadequate for fully independent EV charging due to insufficient solar radiation, the deficit will be supplied by the grid (Figure 4c). In this mode, the grid-interfaced bidirectional converter is in the rectification mode, and the EV-interfaced bidirectional DC–DC converter operates in the buck mode. Because PV generation is variable, the system requires a controller to continuously monitor the power generated by the PV and modify the grid intake accordingly to guarantee that the required power to the EV is maintained.

Mode 4 (PV-to-ESU (PV2ESU)): When there is no EV to be charged, then all the available PV power is directed to the ESU using the PV- and ESU-interfaced DC–DC converters

Energies 2022, 15, 4648 7 of 28

the grid-interface bidirectional converter is in the rectification mode. This mode tends to exploit the chance of a low grid tariff to boost charging station benefits (Figure 4e).

Mode 6 (ESU-to-EV (ESU2EV)): In this mode, the energy stored in the ESU (from the PV modules or the electricity grid) is utilised for EV charging through the ESU- and the EV-interfaced DC–DC converters. This mode assists the grid in charging the EV from the ESU during peak hours, overnight, or during the daytime when the PV power is insufficient to meet the EV demand (Figure 4f).

Mode 7 (PV and ESU-to-EV): When the PV alone is unable to meet the EV's demand and the ESU has adequate SOC, this mode is activated, and the EV is charged by the power from both the PV modules and the ESU. To extract the maximum power from the PV modules, the PV-interfaced DC–DC unidirectional converter is used. Two bidirectional DC–DC converters also interface the ESU and EV. After extracting the maximum available power from the PV modules, the output power (from the PV modules and the ESU) is further conditioned by the DC charger to guarantee that the required power to the EV is retained. This mode also will help to decrease the grid burden caused by EV charging (Figure 4g).

Mode 8 (EV-to-grid (V2G)): EVs can be used as auxiliary power sources and contribute to grid stability during peak demand hours. In this mode, energy is transferred from the EV batteries to the grid via the EV-interfaced bidirectional DC–DC converter and grid-interfaced bidirectional converter. The EV-interfaced and grid-interfaced converters are in the boost and inversion modes, respectively. EV power availability, however, is contingent on the EV driver's willingness to discharge EV batteries into the electricity grid. Furthermore, because this may shorten the lifespan of an electric vehicle's battery, it is not suggested unless the financial gain can be justified. It should be noted that the PV power can also be directed to the grid in this mode as long as there are simultaneous operating conditions of all system components (Figure 4h).

Mode 9 (PV-to-grid (PV2G)): The generated PV power can also be sent directly to the grid ... (Figure 4j).

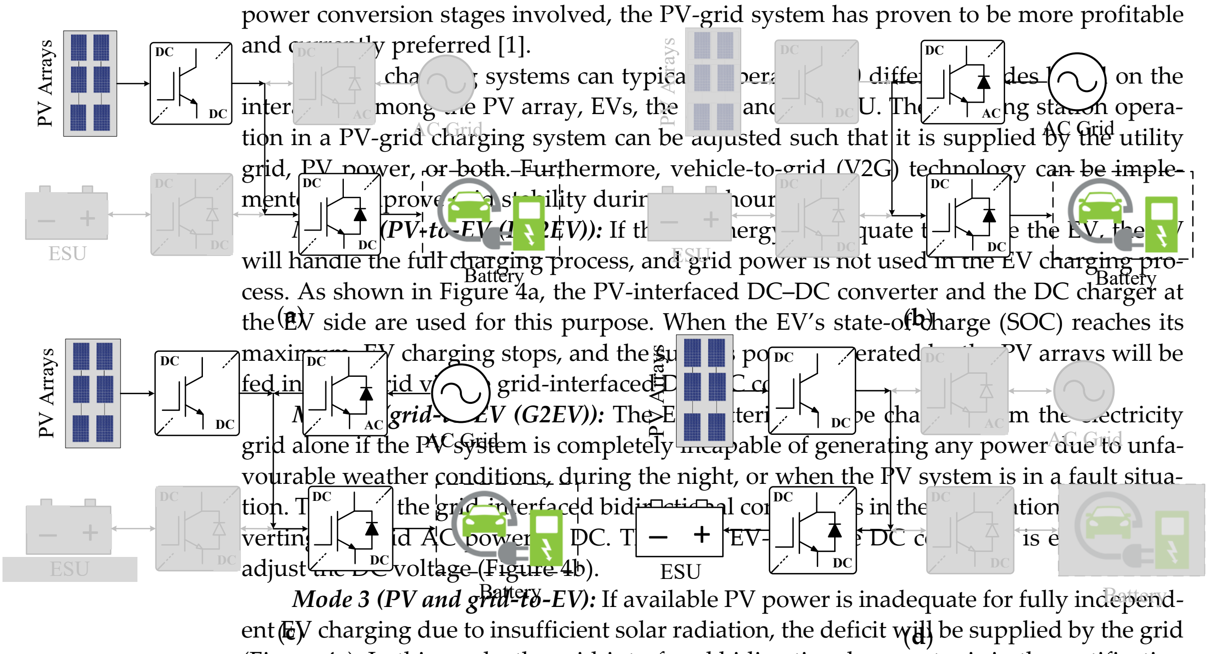

Figure 4. Cont.

Energies **2022**, *15*, 4648 9 of 28

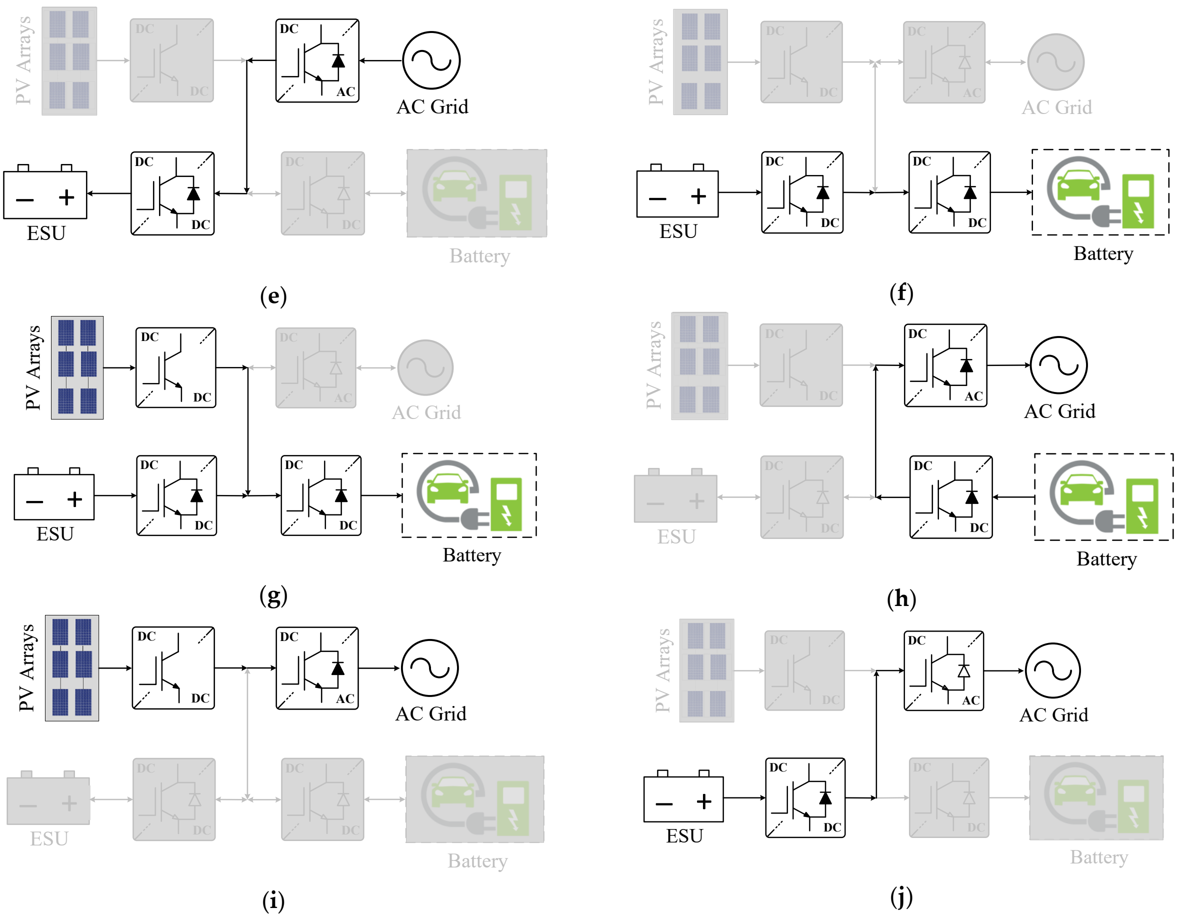

Figure 4. Operating modes of PV-grid charging system: (**a**) Mode 1: PV-to-EV, (**b**) Mode 2: Grid-to-EV, (**c**) Mode 3: PV and grid-to-EV, (**d**) Mode 4: PV-to-ESU, (**e**) Mode 5: Grid-to-ESU, (**f**) Mode 6: ESU-to-EV, (**g**) Mode 7: PV and ESU-to-EV, (**h**) Mode 8: EV-to-grid (V2G), (**i**) Mode 9: PV-to-grid, and (**j**) Mode 10: ESU-to-grid.

Mode 2 (grid-to-EV (G2EV)): The EV batteries will be charged from the electricity grid alone if the PV system is completely incapable of generating any power due to unfavourable weather conditions, during the night, or when the PV system is in a fault situation. To do so, the grid-interfaced bidirectional converter is in the rectification mode, converting the grid AC power to DC. Then, the EV-interface DC converter is employed to adjust the DC voltage (Figure 4b).

Mode 3 (PV and grid-to-EV): If available PV power is inadequate for fully independent EV charging due to insufficient solar radiation, the deficit will be supplied by the grid (Figure 4c). In this mode, the grid-interfaced bidirectional converter is in the rectification mode, and the EV-interfaced bidirectional DC–DC converter operates in the buck mode. Because PV generation is variable, the system requires a controller to continuously monitor the power generated by the PV and modify the grid intake accordingly to guarantee that the required power to the EV is maintained.

Mode 4 (PV-to-ESU (PV2ESU)): When there is no EV to be charged, then all the available PV power is directed to the ESU using the PV- and ESU-interfaced DC–DC converters (Figure 4d). This mode aids the charging system in reducing grid reliance by storing energy in the ESU for later use, particularly during rush hours.

Mode 5 (grid-to-ESU): Power will be directed from the grid to the ESU when the grid is not overloaded, and electricity prices are relatively low (e.g., overnight). In this mode, the grid-interface bidirectional converter is in the rectification mode. This mode tends to exploit the chance of a low grid tariff to boost charging station benefits (Figure 4e).

5. Converter Topologies for PV-Grid Charging Systems

Developments in power conversion technologies play a crucial role in the penetration of solar PV power into EV charging stations. Converter topologies in PV-grid charging stations can be classified as non-integrated and integrated systems [17]. As shown in Figure 3, at least three converters are used in non-integrated architecture. First, a unidirectional DC–DC converter known as a "PV-interfaced converter" is employed for MPPT. The PV-interfaced converter's output is then connected to a second converter known as a "grid-interfaced converter," which typically operates in both rectification and inversion modes. Finally, a bidirectional DC–DC converter known as an "EV-interfaced converter" is utilised to enable EV charging. Each converter has its own controller for efficient charging, which adds to the system's complexity and power losses. Alternatively, a single integrated converter made up of sub-converters can interface the PV, EV, and electricity, as seen in Figure 5. Although additional switches/relays may be added to switch between different modes, the overall integrated system will have fewer total components than its non-integrated counterpart.

Mode 6 (ESU-to-EV (ESU2EV)): In this mode, the energy stored in the ESU (from the PV modules or the electricity grid) is utilised for EV charging through the ESU- and the EV-interfaced DC–DC converters. This mode assists the grid in charging the EV from the ESU during peak hours, overnight, or during the daytime when the PV power is insufficient to meet the EV demand (Figure 4f).

Mode 7 (PV and ESU-to-EV): When the PV alone is unable to meet the EV's demand and the ESU has adequate SOC, this mode is activated, and the EV is charged by the power from both the PV modules and the ESU. To extract the maximum power from the PV modules, the PV-interfaced DC–DC unidirectional converter is used. Two bidirectional DC–DC converters also interface the ESU and EV. After extracting the maximum available power from the PV modules, the output power (from the PV modules and the ESU) is further conditioned by the DC charger to guarantee that the required power to the EV is retained. This mode also will help to decrease the grid burden caused by EV charging (Figure 4g).

Mode 8 (EV-to-grid (V2G)): EVs can be used as auxiliary power sources and contribute to grid stability during peak demand hours. In this mode, energy is transferred from the EV batteries to the grid via the EV-interfaced bidirectional DC–DC converter and grid-interfaced bidirectional converter. The EV-interfaced and grid-interfaced converters are in the boost and inversion modes, respectively. EV power availability, however, is contingent on the EV driver's willingness to discharge EV batteries into the electricity grid. Furthermore, because this may shorten the lifespan of an electric vehicle's battery, it is not suggested unless the financial gain can be justified. It should be noted that the PV power can also be directed to the grid in this mode as long as there are simultaneous operating conditions of all system components (Figure 4h).

Mode 9 (PV-to-grid (PV2G)): The generated PV power can also be sent directly to the grid in two steps, through the PV-interfaced unidirectional DC–DC converter and the grid-interfaced bidirectional converter (in the inversion mode). As this mode is usually operative when the feed-in-tariff rate is substantially high, it results in a financial gain for the owner (Figure 4i).

Mode 10 (ESU-to-grid (ESU2G)): If the ESU has adequate SOC, this mode is operative, and the power saved in the ESU is transferred to the electricity grid in a two-step conversion using the ESU-interfaced bidirectional DC–DC converter in the boost mode and the grid-interfaced bidirectional converter in the inversion mode (Figure 4j).

5. Converter Topologies for PV-Grid Charging Systems

Developments in power conversion technologies play a crucial role in the penetration of solar PV power into EV charging stations. Converter topologies in PV-grid charging stations can be classified as non-integrated and integrated [17]. As shown in Figure 3b, at least three converters are used in non-integrated architectures. First, a unidirectional DC–DC converter known as a "PV-interfaced converter" is employed for MPPT. The PV-interfaced converter's output is then connected to a second converter known as a "grid-interfaced converter," which typically operates in both rectification and inversion modes. Finally, a bidirectional DC–DC converter known as an "EV-interfaced converter" is utilised to enable EV charging. Each converter has its own controller for efficient charging, which adds to the system's complexity and power losses. Alternatively, a single integrated converter made up of sub-converters can interface the PV, EV, and electricity, as seen in Figure 5. Although additional switches/relays may be added to switch between different modes, the overall integrated system will have fewer total components than its non-integrated counterpart.

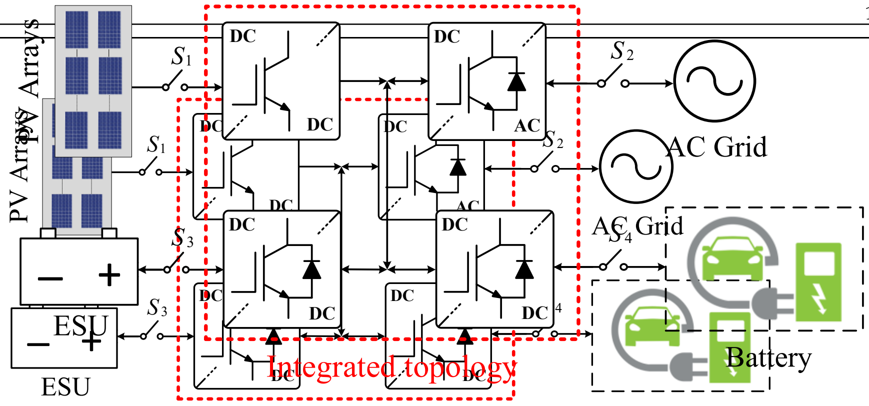

Figure 5. General architecture of integrated topologies for PV-grid EV chargers.

5.1. Non-Integrated Architectures

5.1.1. PV-Interfaced Converter Topologies

A typical commercial PV module has a power rating of 200 W to 300 W and an open-circuit voltage in the range of 20 to 30 Vdc [3]. The PV modules are connected in series to reach higher operating voltage (200–500 Vdc for EV charging applications). A number of strings can be connected in parallel to augment the PV array's power, forming a series-parallel connection. However, nonlinear characteristics (i.e., current-voltage (I-V) and power-voltage (P-V) waveforms) are observed as a result of variations in solar radiation G and ambient temperature T [19,104]. The maximum power point (MPP) is a unique operational point where the power is at its peak at any given time; however, it fluctuates continually by variations in G or T. Therefore, an MPP tracker must be employed to harvest the maximum power from the PV modules, regardless of the weather conditions. Several MPPT methods have been developed in the literature, including intelligent (e.g., Neural Network, Particle swarm optimisation, Fuzzy Logic, Extremum seeking control, etc.) and conventional (Fractional Open-Circuit Voltage, Incremental Conductance, Perturbation, Perturb and Observe (P and O) algorithms, etc.) techniques [105–111]. As shown in Figure 6, the buck-boost or boost topology is mostly utilised as the PV-interfaced DC–DC converter, which adjusts the PV voltage to track the MPP under various operating situations [26,112]. In [7], however, the solar PV array is directly connected to the DC-link. The absence of the unidirectional DC–DC converter reduces one power stage, one of the topology's main advantages. As a result, the converter's circuit complexity and cost are decreased without impacting the PV array's performance.

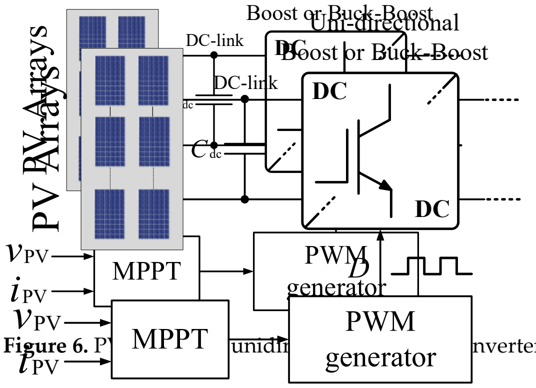

Figure 6. PV-interfaced unidirectional DC–DC converter equipped with MPPT.

5.1.2. EV-Interfaced Converter Topologies

The DC–DC EV-interfaced converter is positioned between the EV battery and the DC-link of a PV system. This converter must be efficient as it can affect the battery life [2]. It adjusts the output voltage of the PV-interfaced converter to the voltage of the EV battery (100–1000 Vdc). High efficiency, bi-directionality, a low input current ripple, a low output

Energies 2022, 15, 4648 11 of 28

It adjusts the output voltage of the PV-interfaced converter to the voltage of the EV battery (100–1000 Vdc). High efficiency, bi-directionality, a low input current ripple, a low output voltage ripple, and soft-switching capabilities are among the key requirements for an EV-interfaced converter [1,113,114]. Bidirectional power flow enables two-way power transfer, allowing the grid to benefit from the energy stored in the EV battery during times of energy shortage. However, the V2G process may shorten the battery lifespan. As a result, it is rarely widely used until cost savings can be justified [2]. Turn-ON and turn-OFF switching losses are significant because the bidirectional DC–DC converter operates at high switching frequencies (kHz range). Thus, soft-switching converters are widely used as EV-interfaced converters [8].

A single-phase bidirectional buck converter shown in Figure 7 can theoretically be employed to charge the EV when the voltage at the input side of the DC–DC converter (output voltage of the PV-interfaced converter) is higher than the voltage required for EV battery charging.

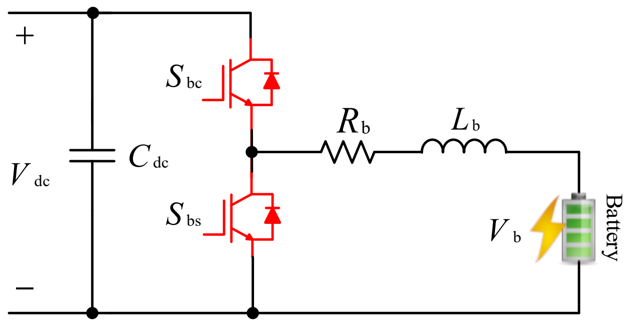

Figure 7. Bidirectional Buck converter as the EV-interfaced converter.

On the other hand, the typical buck converter has two significant drawbacks. First, the DC–DC power stage current ripple must be kept low to reduce the losses associated with the charging and discharging of batteries [2]. Therefore, the inductor of a traditional buck converter is required to be sufficiently large, resulting in a reduction in power density. Second, the converter's power rating is limited because the entire current is followed through only one switch. Therefore, interleaved buck converters (IBCs) with multiple inductors have been developed [77–85]. They offer numerous advantages, including reduced current ripple and inductor size, modularity, increased power, and improved thermal management [2]. Nevertheless, high switching losses, diode recovery losses in high-voltage applications (e.g., EV fast charging), the voltage stress on semiconductor devices, and current equalisation in interleaved converters with a large number of phases are some of the drawbacks of IBC topologies that have been addressed in the literature using proper control strategies such as sliding mode control and gate complementary control [115–117].

Isolation of the EV from all power sources (i.e., the electricity grid and PV) is a requirement for the EV-interfaced converter to meet safety standards (IEC 62955, IEC 61851) [20–23], unless isolation is ensured in the grid-interfaced converter. The low-frequency (LF) transformer (50/60 Hz) connected to the grid and the high-frequency (HF) transformer (50–300 kHz) associated with the DC–DC EV-interfaced converter [118] are two types of galvanic isolation. An LF transformer's isolation needs bulky magnetic components, making the charging station bulky and expensive. Because of the lower installation cost, better power density, and improved reliability, an HF transformer is preferred in the bidirectional DC–DC power stage. The LLC resonant converter [55,56,119–125], dual-active bridge (DAB) converter [57–62], DAB resonant converter [63–72], and phase-shifted full-bridge (PSFB) converter [73–76] are examples of isolated DC–DC converters proposed in publications. Modulation techniques and control methods for isolated DC–DC converters can be complicated. Therefore, non-isolated topologies have been developed in [26,126–129]. Examples of isolated and non-isolated DC–DC converter topologies that can be adopted as the EV-interfaced converter, along with their main features, are shown in Figures 8 and 9, and their main features are listed in Table 3.

Energies **2022**, *15*, 4648 12 of 28

be adopted as the EV-interfaced converter, along with their main features, are shown in Figures 8 and 9, and their main features are listed in Table 3.

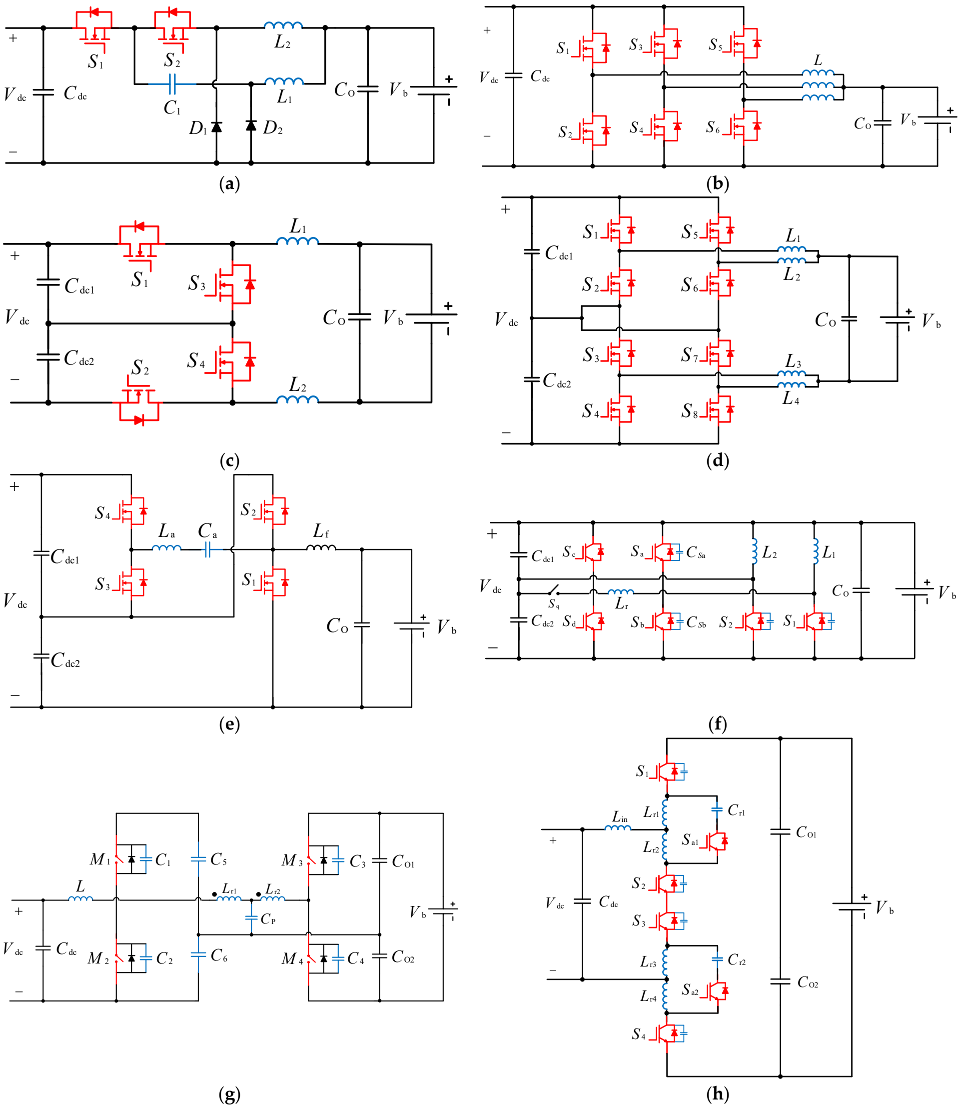

Figure 8. Non-isolated DC–DC converters as the EV-interfaced converter: (**a**) 2-phase interleaved Buck converter (IBC), (**b**) 3-phase IBC, (**c**) 3-level asymmetrical voltage source converter, (**d**) parallel 3-level buck converter, (**e**) zero voltage transition (ZVT) converter, (**f**) interleaved ZVT, (**g**) half-bridge ZVT, and (**h**) 3-level ZVT.

Figure 8. Non-isolated DC–DC converters as the EV-interfaced converter: (a) 2-phase interleaved Buck converter (IBC), (b) 3-phase IBC, (c) 3-level asymmetrical voltage source converter, (d) parallel 3-level buck converter, (e) zero voltage transition (ZVT) converter, (f) interleaved ZVT, (g) half-bridge ZVT, and (h) 3-level ZVT.

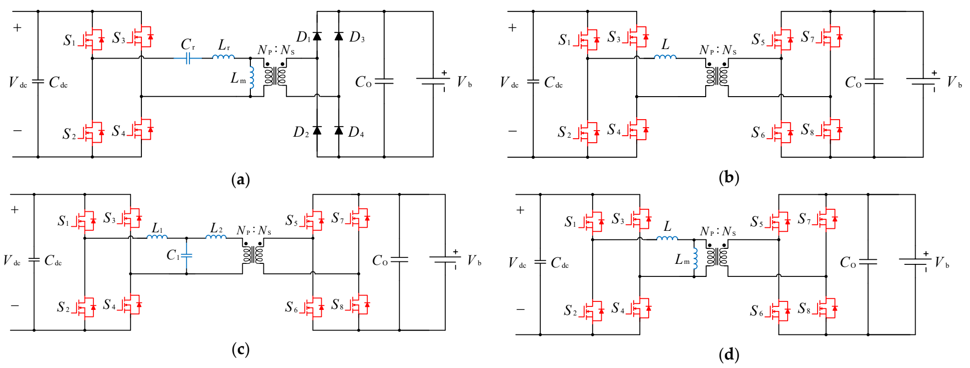

Figure 9. Isolated DC–DC converters as the EV-interfaced converter: (**a**) Full-bridge 3-level LLC resonant converter, (**b**) dual-active bridge (DAB) converter, (**c**) dual-active bridge (DAB) LCL resonant converter, and (**d**) phase-shifted full-bridge (PSFB) converter.

Figure 9. Isolated DC–DC converters as the EV-interfaced converter: (a) Full-bridge 3-level LLC resonant converter, (b) dual-active bridge (DAB) converter, (c) dual-active bridge (DAB) LCL resonant converter, and (d) phase-shifted full-bridge (PSFB) converter.

Table 3. Non-isolated and isolated DC-DC EV-interfaced topologies

Type	Ref.	Figure	Topology	No. of S/D	Voltage/ Power	η	Specifications: Advantages	Specifications: Disadvantages
	[26]	Figure 7	1-phase Buck	2 switches	250 V/48 kW	-	Simple structure and control/V2G support	Large inductor/Low power density/Limited power rating/Absence of isolation/No soft-switching
	[77]	Figure 8a	2-phase Interleaved Buck converter	2 switches 2 diodes	150–200 V	Up to 96%	Reduced switching losses/Lower voltage stress on the semiconductor devices/Reduced current rip-	Sensitivity of current equalization among the phases to duty cycle fluctuation/Ab-

Table 3. Non-isolated and isolated DC–DC EV-interfaced topologies.

Type	Ref.	Figure	Topology	No. of S/D	Voltage/Power	η	Specifications	
							Advantages	Disadvantages
Non-isolated	[26]	Figure 7	1-phase Buck	2 switches	250 V/48 kW	-	Simple structure and control/V2G support	Large inductor/Low power density/Limited power rating/Absence of isolation/No soft-switching
	[77]	Figure 8a	2-phase Interleaved Buck converter (IBC)	2 switches 2 diodes	150–200 V	Up to 96%	Reduced switching losses/Lower voltage stress on the semiconductor devices/Reduced current ripple/Compact structure/Better step-down voltage ratio	Sensitivity of current equalization among the phases to duty cycle fluctuation/Absence of isolation/No soft-switching/No V2G support
	[78]	Figure 8b	3-phase Interleaved Buck converter (IBC)	6 switches (each module)	200–800 V/ Up to 150 kW	-	Increased power/Low cost simple design/Balanced power-sharing among the phases/Modularity/Low input and output current ripple/Minimized inductor size by operating in the discontinuous mode (DCM)/Soft-switching/V2G support	Different phase characteristics (such as power losses and RMS current) among the interleaved phases/Sensitivity of current equalization among the phases to duty cycle fluctuation/Soft-switching would be difficult at higher switching frequencies/Absence of isolation
	[82]	Figure 8c	3-level asymmetrical voltage source converter	4 switches	200–500 V/40 kW	-	Lower rated switches/High-frequency operation/Smaller inductor/Reduced price and size/Compact structure/V2G support/Lower output and inductor current ripples	Absence of isolation/No soft-switching
	[84]	Figure 8d	Parallel 3-level buck converter	8 switches	1.2 kW	-	Can operate with a bipolar DC bus/Compact structure/V2G support	High voltage ripple at the input side/High circulating current/Absence of isolation/No soft-switching
	[126]	Figure 8e	Zero voltage transition (ZVT) converter	4 switches	220 V	-	High voltage conversion ratio/Compatible with different voltage ranges/Reduced voltage ripple with interleaved design/Soft-switching/V2G support	High conduction power losses because the resonant circuit is positioned in the current path)/Absence of isolation
	[127]	Figure 8f	Interleaved ZVT	6 switches	70–400 V/1 kW	~95%	Low conduction losses/Low input current ripple/Small size inductors/Interleaved design/Soft-switching	High power losses at high power applications/Reverse recovery loss of body diodes/Absence of isolation/No V2G support
	[128]	Figure 8g	Half-bridge ZVT	4 switches	250 V/100 W	-	Capable of operating at moderate duty-cycle ratio/Lower EMI/Reduced voltage stresses on switches/ Compact structure/ Relatively simple control/Soft-switching/V2G support	Limited soft-switching range/Increased losses when operating at high switching frequencies/More components in the current path/Longer conduction path/Low efficiency/Absence of isolation
	[129]	Figure 8h	3-level ZVT	6 switches	~300 V/100 kW	98%	Reduced voltage stresses on semiconductor devices, so suitable for medium and very high-power applications/Soft-switching/ V2G support	More resonant circuits/increased probability of losing soft-switching/High losses at light loads/Large size and the volume of the circuit/High control complexity

Table 3. *Cont.*

Type	Ref.	Figure	Topology	No. of S/D	Voltage/Power	η	Specifications	
							Advantages	Disadvantages
Isolated	[121]	Figure 9a	Full-bridge 3-level LLC resonant converter	6 switches 6 diodes	225–378 V/6.6 kW	98.14%	Good voltage regulation/Can operate with light loads/No diode recovery losses/A single capacitor to filter the output side/Compact size/Low EMI/High efficiency/Soft-switching	Unidirectional power flow/Complex design procedure/Switching and resonant frequencies are close/No V2G support
	[57]	Figure 9b	Dual-active bridge (DAB) converter	8 switches	200–450 V/20 kW	96%	High efficiency/High power density/Galvanic isolation/Soft-switching/V2G support/Modular design/Wide range of voltage transfer ratio	Soft-switching is challenging at light to medium EV battery voltage/Transformer peak current losses/Transformer's operation in saturation/Current overshoot/High losses/High-frequency current ripple, reducing battery lifetime
	[63]	Figure 9c	Dual-active bridge (DAB) LCL resonant converter	8 switches	400 V/4 kW	95%	Reduced reactive power/Increased efficiency/Reduced conduction loss compared to DAB converter/No transformer saturation/V2G support	Cannot guarantee soft-switching for a wide range of battery voltage/Complex synchronization and control/High cost
	[75]	Figure 9d	Phase-shifted full-bridge (PSFB) converter	4 switches 6 diodes	270–420 V/3.3 kW	98.5%	Modular design/Reduced stresses on semiconductor devices/reduced Electro magnetic interference/No circulating current on primary and secondary sides/Soft-switching	Hard switching for secondary side diodes/Low efficiency/Severe voltage overshoot across the full-bridge rectifier due to high-voltage EV charging/Reverse recovery problems of the diodes for high power flow/No V2G support

Energies 2022, 15, 4648 15 of 28

5.1.3. Grid-Interfaced Converter Topologies

The grid-interfaced converter controls power transfer from the utility grid to the EV battery charger. Depending on the current flow direction, this converter can operate either in the rectification (AC–DC) or inversion (DC–AC) mode, delivering power from the grid to the EV or feeding it back into the grid (under V2G mode), respectively [9]. Further, during the daytime and when there is no EV to be charged, this converter can be used to transfer the available PV power into the grid. Bi-directionality, high-power density, low total harmonic distortion (THD), galvanic isolation, and high efficiency are the primary converter requirements [26]. The bidirectional voltage source inverter (VSI) shown in Figure 10 has been the most commonly used converter in the literature as the grid-interfaced converter [19]. Depending on the output voltage, this converter can operate as a step-down (buck) [28–38,56–58] or (boost) [43–45] converter. However, the conventional VSI suffers from low efficiency. Other potential topologies with higher efficiencies include SWISS [27,39,41] and VIENNA converters [40,42,54] (See Figure 11). Moreover, the SOC of the EV batteries with a capacity of 20 kWh–40 kWh must reach 80% within 30 min. The output power of the converters can be stacked to satisfy the requirements of EV chargers using a modular approach [130,131]. Therefore, in EV fast and ultra-fast charging applications, multilevel converters (MLCs), including Cascaded H-Bridge (CHB) [46,47], Flying Capacitor (FC) [48,49], and Neutral Point Clamped (NPC) [50–53] converters have been preferable in some publications (see Figure 12). Their outstanding advantages include low THD, smaller dv/dt, minimized magnetic components, less voltage stress across the semiconductor devices in high-voltage applications (e.g., 100 V-rated switches within the 400 V-voltage battery range), low electromagnetic interference (EMI), and a low rated switch, in addition to reduced voltage transition between levels [132–143]. However, reliability, voltage balancing, high cost, and complex structure and control are some concerns related to MLCs. A technical comparison among examples of grid-interfaced converters is presented in Table 4. Grid-connected converters inject harmonics into the grid, degrading power quality. In order to ensure that input sinusoidal currents are in phase with grid voltages, power factor correction (PFC) solutions have been developed in the literature [2].

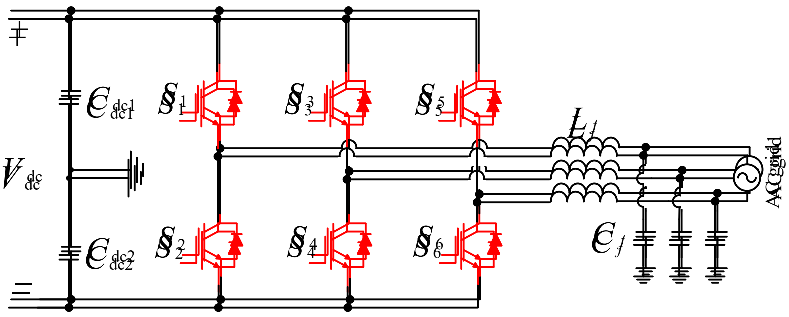

Figure 10. Bidirectional voltage source inverter (VSI) as the grid-interfaced converter.

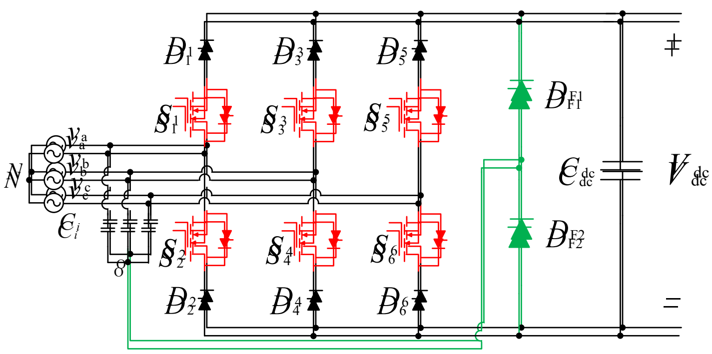

(a)

Figure 11. *Cont.*

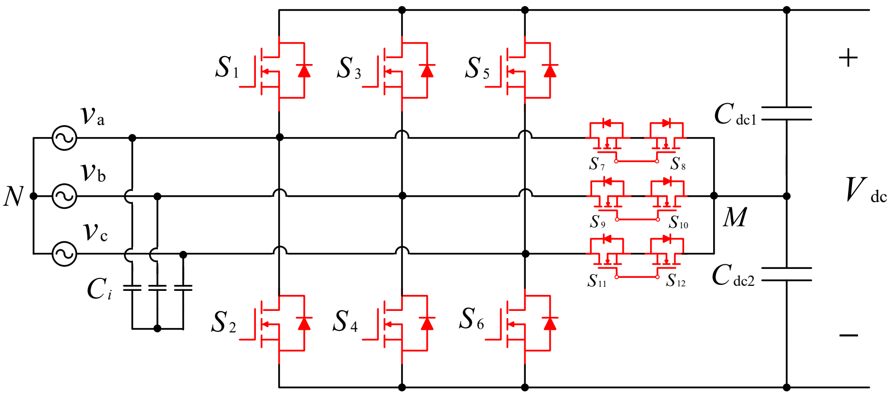

(b)

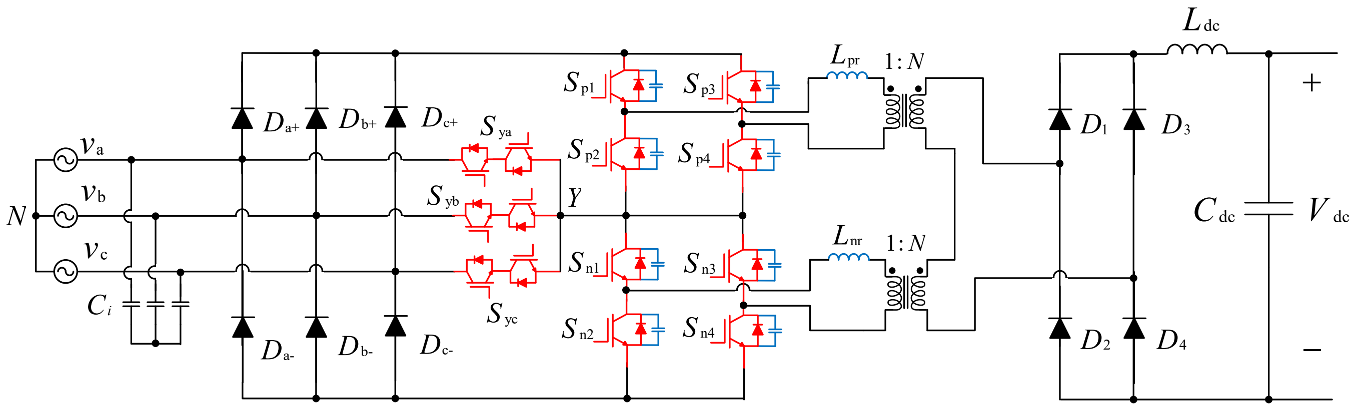

(c)

Figure 11. Grid-interfaced topologies: (**a**) Three-phase modified Buck type converter, (**b**) VIENNA converter, and (**c**) SWISS converter.

Table 4. A technical comparison among grid-interfaced converter topologies.

Type		Ref.	Figure	No. of S/D	Rectification/Inversion Mode	Voltage/Power	THD	η	Specifications: Advantages	Specifications: Disadvantages
Voltage source Inverter (VSI)	Step-up (Boost mode)	[45]	Figure 10	6 Switches	Both	620 V/4 kW	3.29%	96.5%	Simplified structure and control scheme/Continuous input current/High output DC voltage/Low current stress/Low THD/High efficiency/Soft-switching	Harmonics appear at the DC-link voltage under unbalanced/AC input voltage/High switching losses
	Step-down (Buck mode)	[31]	Figure 11a	6 Switches 8 diodes	Rectification	400 V		~97%	Simplified structure and control scheme/Continuous input current/High output DC voltage/Low current stress/Low THD/High efficiency/Minimized reverse recovery losses of the anti-parallel diodes/Soft-switching	Semiconductor losses/High voltage stresses on the switches in EV charging/Input current distortion, especially at light load conditions/Complex control/Reduced soft-switching capability

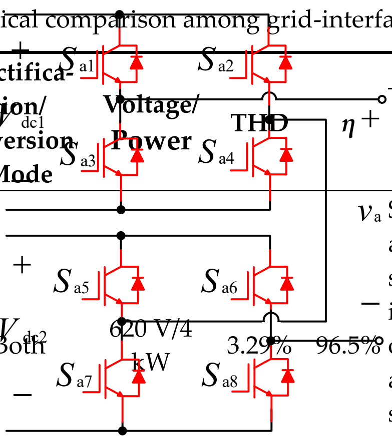

(a)

Figure 12. *Cont.*

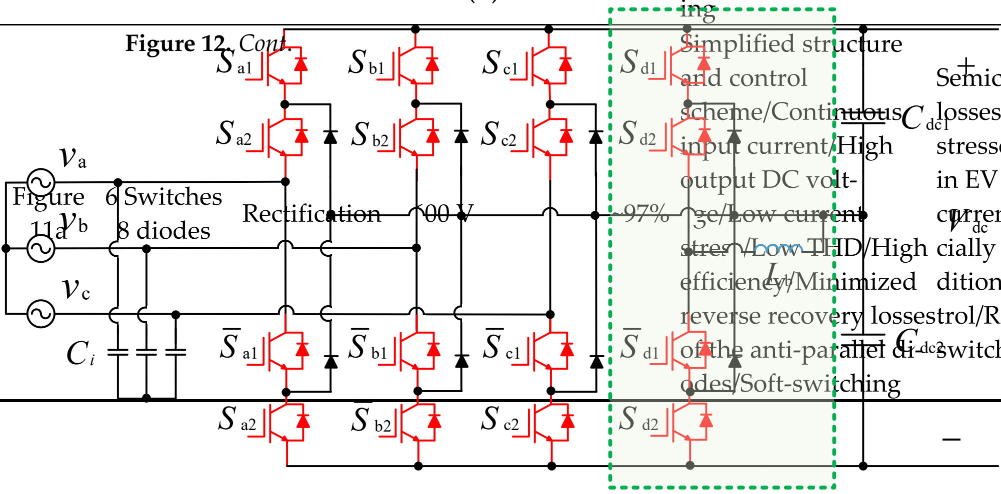

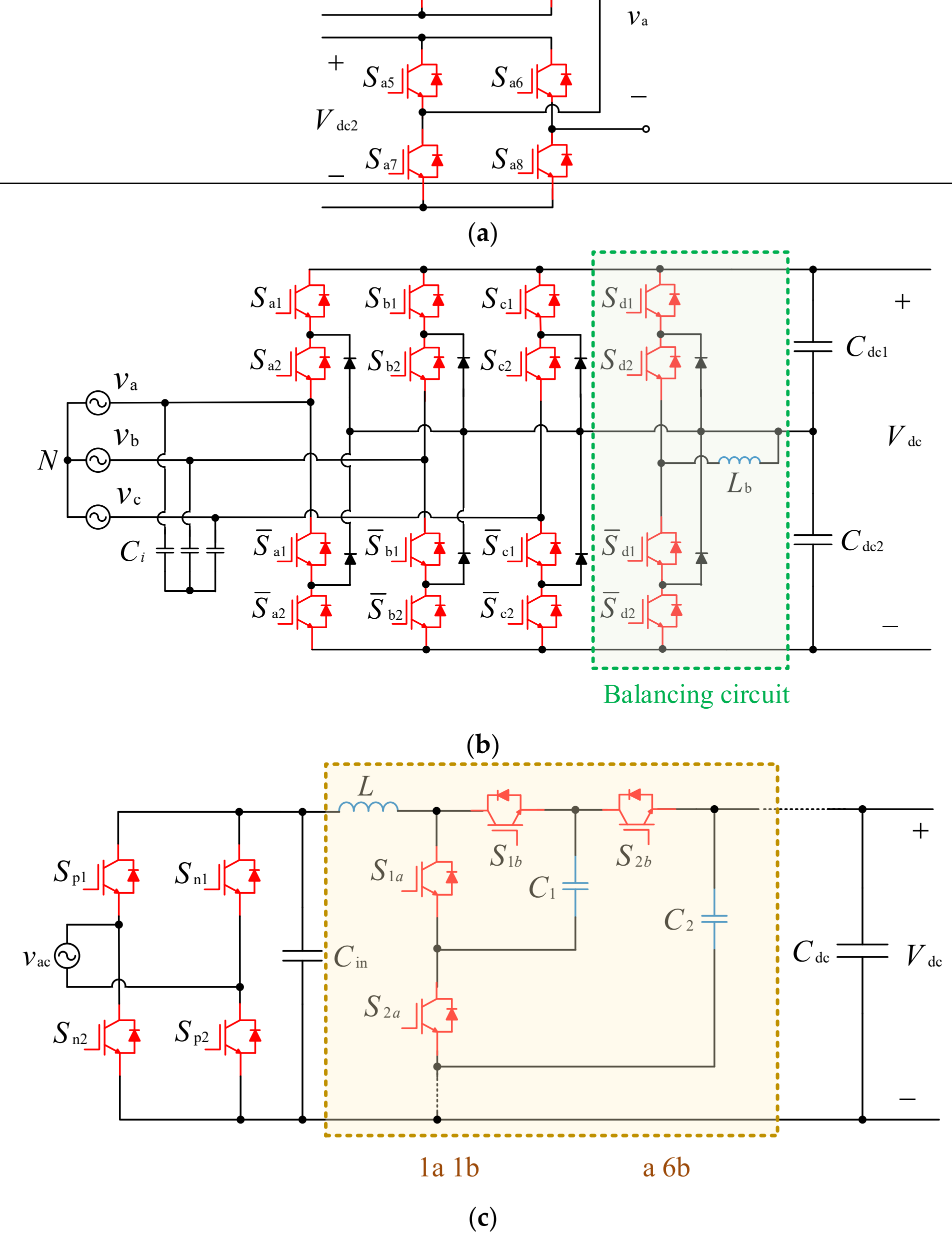

Figure 12. Multilevel converters (MLCs) used as grid-interfaced converter (**a**) Cascaded H-Bridge (CHB), (**b**) Neutral Point Clamped (NPC), and (**c**) Flying Capacitor (FC).

5.2. Integrated Architectures

The main disadvantage of non-integrated architectures for EV charging is the requirement to control at least three converters, namely, the PV-interfaced DC–DC converter for the MPPT algorithm, the single/three-phase grid-connected converter, and the EV-interfaced DC–DC converter for the battery's charging. Therefore, non-integrated architectures suffer from increased complexity and high power losses. Alternately, multi-port integrated topologies for EV charging can integrate EV (or ESU), PV, and the grid using one single-stage power conversion system alone, resulting in higher power density, smaller-scale communication infrastructure requirements, lower cost, and higher efficiency as a result of a reduced number of power stages [18,86–89].

Examples of existing multi-port integrated architectures for EV charging are reviewed next, with a technical comparison presented in Table 5.

Table 4. A technical comparison among grid-interfaced converter topologies.

Type		Ref.	Figure	No. of S/D	Rectification/ Inversion Mode	Voltage/Power	THD	η	Specifications	
									Advantages	Disadvantages
Voltage source Inverter (VSI)	Step-up (Boost mode)	[45]	Figure 10	6 Switches	Both	620 V/4 kW	3.29%	96.5%	Simplified structure and control scheme/Continuous input current/High output DC voltage/Low current stress/Low THD/High efficiency/Soft-switching	Harmonics appear at the DC-link voltage under unbalanced/AC input voltage/High switching losses
	Step-down (Buck mode)	[31]	Figure 11a	6 Switches 8 diodes	Rectification	600 V	-	~97%	Simplified structure and control scheme/Continuous input current/High output DC voltage/Low current stress/Low THD/High efficiency/Minimized reverse recovery losses of the anti-parallel diodes/Soft-switching	Semiconductor losses/High voltage stresses on the switches in EV charging/Input current distortion, especially at light load conditions/Complex control/Reduced soft-switching capability
VIENNA converter		[42]	Figure 11c	12 Switches	Both	800 V/15 kW	<5%	>98%	Suitable for high power applications/Simple structure and control method/High power Density and efficiency/Low THD/Neutral connection-free structure/Low voltage stresses on the switches/Consistent with bipolar DC bus/Soft-switching/operating at unity power factor	The need for dc-link capacitors/Limited switching frequency for a better trade-off between high efficiency and high-power density
SWISS converter		[39]	Figure 11b	14 Switches 10 diodes	Rectification	400 V/10 kW	<3%	95%	High efficiency/Low common-mode noise/Low conduction and switching loss	Complex circuit and control in high power levels/Unidirectional power flow/Reduced soft-switching capability
Multilevel	CHB	[46]	Figure 12a	8 Switches (per phase)	Both	540 V/2 kW	Low	95.4 %	Several switching states/Modularity/Capability to isolate the faulty cells without any interruption in operations/Low current ripple/Robustness/ Easy implementation	Capacitors voltage balancing/Inadequacy of delivering maximum modulation index/Vulnerability to potential failure/Reliability/No soft-switching
	NPC	[51]	Figure 12b	16 switches 8 diodes	Both	~450 V/3.6 kW	5.39%	-	Less distortion in output voltage waveforms/Decreased stresses on switches/Low THD/Minimised switching losses/Improved reliability/Consistent with bipolar DC bus structure	Severe unbalancing problem caused by uncertainties (e.g., various battery technologies and random arrival of vehicles/Limited switching frequency/Limited maximum phase current/Complex control/No soft-switching
	FC	[48]	Figure 12c	8 switches (per level)	Both	400 V/1.5 kW	<3.5%	~99%	High-frequency operation/Smaller passive components/High power delivery capability (in three-phase)	High cost/Challenges in PFC/No soft-switching

Table 5. A technical comparison between integrated architectures.

Ref.	Figure	Sub-Converters			Power Range	Operating Modes	η	Specifications	
		EV-Interfaced Converter	Grid-Interfaced Converter	PV-Interfaced Converter				Advantages	Disadvantages
[18]	Figure 13	Interleaved Flyback	Three-phase VSI	Interleaved boost	10 kW	V2G, PV2EV, PV2G, G2V	~95%	High power density/Modularity/Electrical isolation/High Switching frequency/High partial and peak load efficiency	Hard switching for the interleaved PV-interfaced and three-phase VSI/Complex controls for the three sub-converters/Reliability concerns/No ESU/No control over SOC of the EV batteries/Soft-switching for EV-interfaced converter only
[86]	Figure 16	Half-bridge	Full-bridge	Half-bridge	3.5 kW	V2G, PV2EV, PV2G, G2V	-	V2G support/Low THD/Simple structure/High power density/Unity power factor	No ESU/No electrical isolation/Hard switching/No soft-switching
[88]	Figure 14	Bidirectional DC–DC converter	Bidirectional AC–DC converter	Unidirectional Boost	-	V2G, PV2EV, PV2G, G2V, PV2ESU, ESU2G, ESU2EV, G2ESU	-	Electrical isolation/Modularity/A wide variety of DC sources are supported through a multi winding transformer	Hard switching for the PV-, EV-, and grid-interfaced sub-converters, particularly in high power applications/Challenging transformer design for high power flow/Soft-switching for TAB converter only
[89]	Figure 15	Interleaved Boost	Dual-active bridge (DAB)	Interleaved Boost	0.2 kW	V2G, PV2EV, PV2G, G2V	~96%	Simple and Compact design/No complex control or optimization for the modulation technique/High power density/It can be scaled up to high power levels	No ESU/Hard switching for the interleaved Boost converter/Large output filter is required to secure low THD/Soft-switching for DAB converter only

vide bidirectional power flow capability, a DC–DC unidirectional boost converter for the PV port, and a bidirectional converter to interface with the utility grid. The proposed topology offers electrical isolation and modularity. It could be more advantageous by supporting a wide range of DC sources utilising a multi-winding transformer. However, although soft-switching is guaranteed for the TAB converter, the three sub-converters suffer from hard switching, particularly in high-power applications.

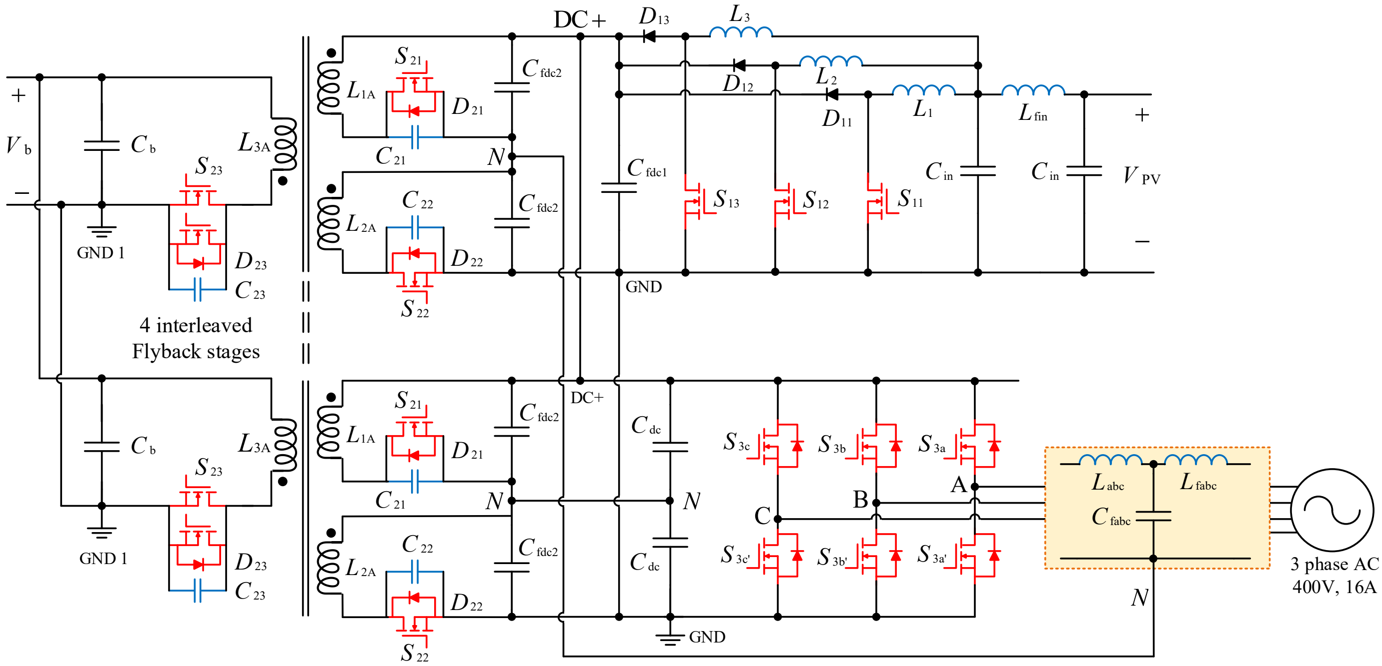

Figure 13. Three-port integrated architecture for EV charging, including a unidirectional DC–DC interleaved boost topology for the PV port, a bidirectional three-phase VSI for the grid port, and a bidirectional isolated interleaved DC–DC Flyback topology for EV side [18].

Energies 2022, 15, 4648 20 of 28

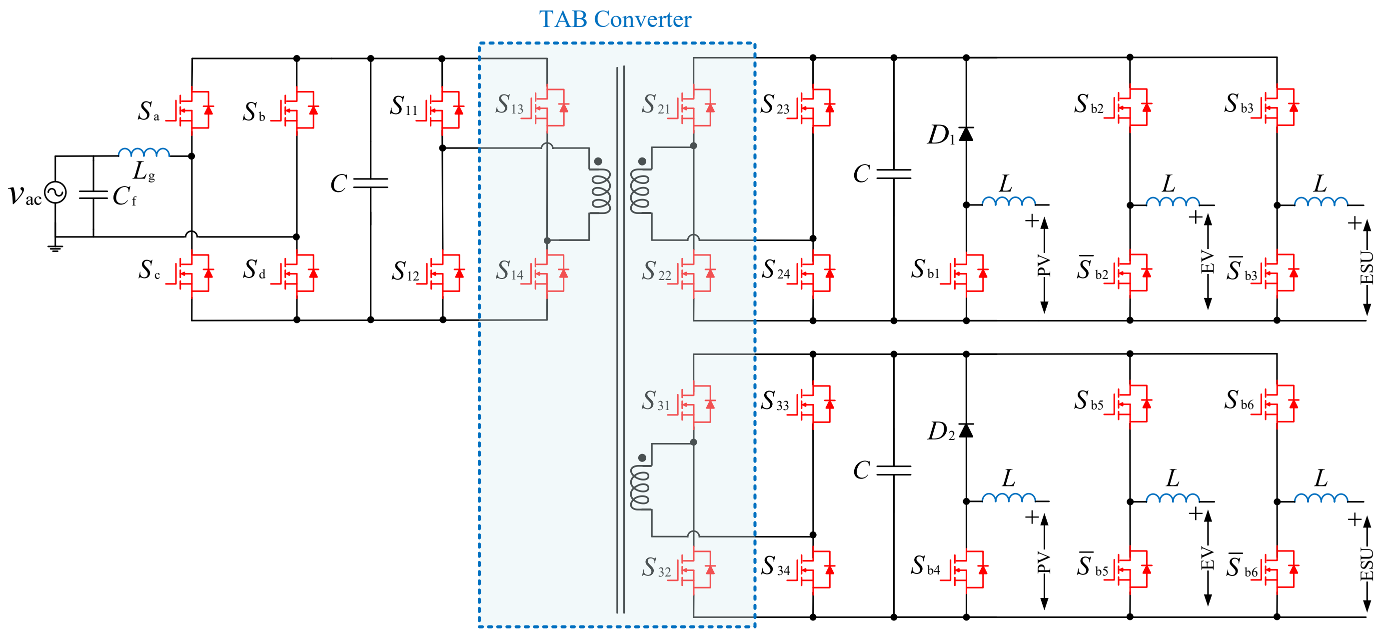

Figure 14. Four-port integrated architecture for EV charging, including a triple active bridge (TAB) converter, a bidirectional DC–DC converter interfacing the EV battery, a DC–DC unidirectional boost converter for PV port, and a bidirectional grid-interfaced converter [88].

A three-port integrated topology based on interleaved Boost and DAB converters has been proposed in [89]. As shown in Figure 15, the DAB topology interfaces with the grid (Port-3) while the interleaved boost converter interfaces EV (Port-1) and PV (Port-2). Apart from a simple and compact design, the modulation technique used does not require complex control or optimization. Furthermore, the proposed architecture offers high power density and can be scaled up to higher power. Despite inherent soft-switching for the DAB converter, the interleaved Boost converter suffers from hard switching, plus a large output filter is required to secure low THD.

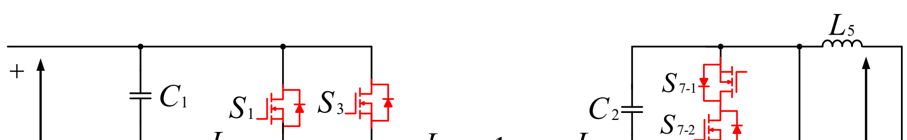

been proposed in [89]. As shown in Figure 15, the DAB topology interfaces with the grid (Port-3) while the interleaved boost converter interfaces EV (Port-1) and PV (Port-2). Apart from a simple and compact design, the modulation technique used does not require complex control or optimization. Furthermore, the proposed architecture offers high power density and can be scaled up to higher power. Despite inherent soft-switching for the DAB converter, the interleaved Boost converter suffers from hard switching, plus a large output filter is required to secure low THD.

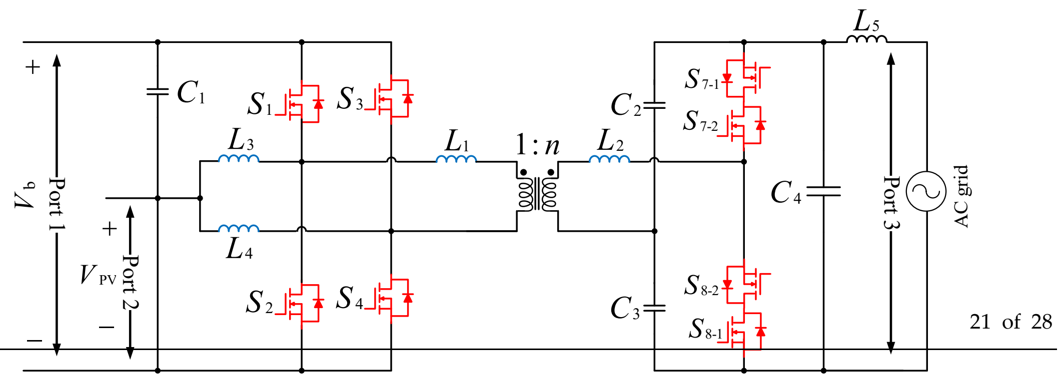

Figure 15. Three-port integrated architecture for EV charging, including a DAB converter to interface the grid and an interleaved Boost converter to interface with EV and PV (Port 3: Grid, port 1: EV, port 2: PV) [89].

and the absence of isolation are its main drawbacks, which cannot be ignored in EV charging systems [89].

A three-port integrated topology interfacing PV, EV, and the electricity grid has been presented in [86]. As shown in Figure 16, the proposed topology includes an A–DC bidirectional full-bridge converter interfacing with the electricity grid, a DC–DC bidirectional half-bridge converter on the EV side, and a DC–DC unidirectional half-bridge converter at the PV port. The V2G support, low THD, simple structure, high power density, and unity power factor are the benefits delivered by this topology. However, hard switching

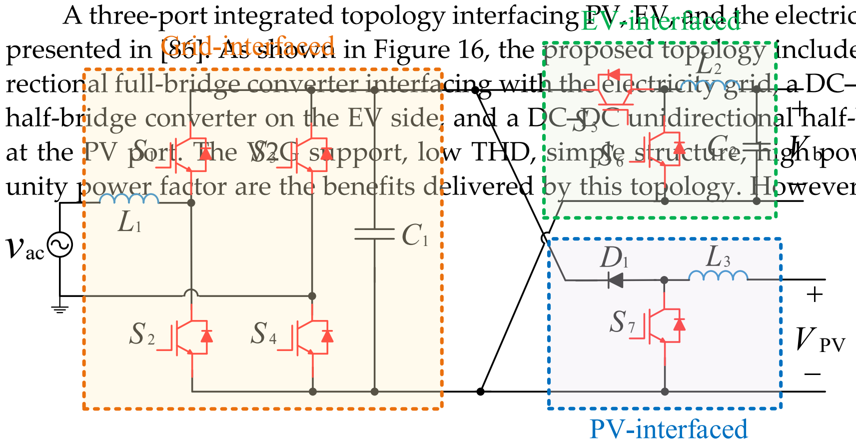

Figure 16. Three-port integrated architecture for EV charging with an AC–DC bidirectional full-bridge converter to interface with the grid, a DC–DC bidirectional half-bridge converter at EV side, and a DC–DC unidirectional half-bridge converter for the PV port [86].

Table 5. A technical comparison between integrated architectures.

Ref.	Figure	Sub-Converters: EV-Interfaced Converter	Sub-Converters: Grid-Interfaced Converter	Sub-Converters: PV-Interfaced Converter	Specifications: Power Range	Specifications: Operating Modes	Specifications: η	Advantages	Disadvantages
[18]	Figure 13	Interleaved Flyback	Three-phase VSI	Interleaved boost	10 kW	V2G, PV2EV, PV2G, G2V	~95%	High power density/Modularity/Electrical isolation/High Switching frequency/High partial and peak load efficiency	Hard switching for the interleaved PV-interfaced and three-phase VSI/Complex controls for the three sub-converters/Reliability concerns/No ESU/No control over SOC of the EV batteries/Soft-switching for EV-interfaced converter only
[86]	Figure 16	Half-bridge	Full-bridge	Half-bridge	3.5 kW	V2G, PV2EV, PV2G, G2V	-	V2G support/Low THD/Simple structure/High power density/Unity power factor	No ESU/No electrical isolation/Hard switching/No soft-switching
	Figure	Bidirectional	Bidirectional	Unidirectional		V2G, PV2EV, PV2G, G2V, PV2ESU		Electrical isolation/Modularity/A wide variety of DC	Hard switching for the PV-, EV-, and grid-interfaced sub-converters, particularly in high power applica-

A 10 kW three-port EV charger consisting of a unidirectional DC–DC power stage based on an interleaved boost topology for the PV port, a bidirectional three-phase VSI for the grid port, and a bidirectional isolated DC–DC converter based on an interleaved Flyback topology for the EV side, is presented in [18] (see Figure 13). Bidirectional power flow (V2G support), high power density, modularity, electrical isolation, and quasi-resonant soft-switching for the Flyback topology are some of the merits of this integrated topology. Further, interleaving, high switching frequency, and silicon carbide (SiC) power devices have made this topology capable of delivering high partial and peak load efficiency. However, soft-switching is not maintained for the interleaved PV-interfaced and the three-phase VSI. Complex controls are implemented for the three sub-converters, but there is no control over the SOC of the EV batteries.

An isolated four-port topology integrating PV, a grid, energy storage, and EV is presented in [88]. As shown in Figure 14, the sub-converters include a triple active bridge (TAB) converter, a bidirectional DC–DC converter interfacing with the EV battery to provide bidirectional power flow capability, a DC–DC unidirectional boost converter for the PV port, and a bidirectional converter to interface with the utility grid. The proposed topology offers electrical isolation and modularity. It could be more advantageous by supporting a wide range of DC sources utilising a multi-winding transformer. However, although soft-switching is guaranteed for the TAB converter, the three sub-converters suffer from hard switching, particularly in high-power applications.

A three-port integrated topology based on interleaved Boost and DAB converters has been proposed in [89]. As shown in Figure 15, the DAB topology interfaces with the

Energies 2022, 15, 4648 21 of 28

grid (Port-3) while the interleaved boost converter interfaces EV (Port-1) and PV (Port-2). Apart from a simple and compact design, the modulation technique used does not require complex control or optimization. Furthermore, the proposed architecture offers high power density and can be scaled up to higher power. Despite inherent soft-switching for the DAB converter, the interleaved Boost converter suffers from hard switching, plus a large output filter is required to secure low THD.

A three-port integrated topology interfacing PV, EV, and the electricity grid has been presented in [86]. As shown in Figure 16, the proposed topology includes an A–DC bidirectional full-bridge converter interfacing with the electricity grid, a DC–DC bidirectional half-bridge converter on the EV side, and a DC–DC unidirectional half-bridge converter at the PV port. The V2G support, low THD, simple structure, high power density, and unity power factor are the benefits delivered by this topology. However, hard switching and the absence of isolation are its main drawbacks, which cannot be ignored in EV charging systems.

6. Future Research

The EV charging system faces challenges when PV-based EV chargers are integrated into the grid. EV batteries are usually used to decrease the problems associated with the PV variable nature and electricity grid faults, which result in unwanted charging or discharging of EV batteries. This can shorten the lifespan of EV batteries. Therefore, aside from adopting a proper integrated or non-integrated topology in EV charging stations, there is an essential requirement for a reliable, effective, and uncomplicated controller capable of meeting EV user requirements, supporting the four-quadrant operation of the EV charger for G2V/V2G, mitigating grid current harmonics, supporting the electricity grid with reactive power, dealing with the intermittent nature of renewables, and charging the EVs from RES with seamless transitions between operating modes. Various control algorithms with their pros and cons have been proposed in the literature, such as model predictive control (MPC), heuristic optimizations, fuzzy logic control (FLC), and particle swarm optimization (PSO). A comparison study representing the associated control methods could provide a better direction for future research.

7. Conclusions

PV-EV charging systems, including PV stand-alone (off-grid) and PV-grid (on-grid) infrastructures, have been discussed in this paper. Although the off-grid infrastructure involves fewer power stages, its on-grid counterpart is preferred to ensure a consistent electricity supply for charging EVs during insufficient solar PV power periods. Adopted power converters for on-grid infrastructures were divided into non-integrated and integrated topologies. Non-integrated topologies require at least three power converters, namely, PV-interfaced, grid-interfaced, and EV-interfaced converters, whereas one single converter is interfaced with PV, grid, and EV in integrated topologies. Soft-switching, isolation, low input and output current/voltage ripple, high efficiency, and high power density are key requirements for the converters used in EV charging systems. Bidirectional power flow is needed for the EV- and grid-interfaced converters to increase grid stability during peak load hours.

Author Contributions: Conceptualization, A.D. and B.W.W.; methodology, F.N.E., A.D. and B.W.W.; software, F.N.E. and A.D.; validation, F.N.E. and A.D.; formal analysis, F.N.E., A.D. and B.W.W.; investigation, F.N.E., A.D. and B.W.W.; resources, F.N.E., A.D. and B.W.W.; data curation, F.N.E., A.D. and B.W.W.; writing—original draft preparation, F.N.E.; writing—review and editing, A.D. and B.W.W.; visualization, F.N.E., A.D. and B.W.W.; supervision, A.D.; project administration, A.D.; funding acquisition, A.D. All authors have read and agreed to the published version of the manuscript.

Funding: This research received no external funding.

Institutional Review Board Statement: Not applicable.

Informed Consent Statement: Not applicable.

Data Availability Statement: Not applicable.

Conflicts of Interest: The authors declare no conflict of interest.

References

1. Khan, S.; Ahmad, A.; Ahmad, F.; Shafaati Shemami, M.; Saad Alam, M.; Khateeb, S. A comprehensive review on solar powered electric vehicle charging system. *Smart Sci.* **2018**, *6*, 54–79. [CrossRef]
2. Safayatullah, M.; Elrais, M.T.; Ghosh, S.; Rezaii, R.; Batarseh, I. A Comprehensive Review of Power Converter Topologies and Control Methods for Electric Vehicle Fast Charging Applications. *IEEE Access* **2022**, *10*, 40753–40793. [CrossRef]
3. Bhatti, A.R.; Salam, Z.; Abdul, M.J.B.; Yee, K.P. A comprehensive overview of electric vehicle charging using renewable energy. *Int. J. Power Electron. Drive Syst.* **2016**, *7*, 114. [CrossRef]
4. *Global EV Outlook*; International Energy Agency: Paris, France, 2021.
5. Adhikari, M.; Ghimire, L.P.; Kim, Y.; Aryal, P.; Khadka, S.B. Identification and analysis of barriers against electric vehicle use. *Sustainability* **2020**, *12*, 4850. [CrossRef]
6. Krishna, G. Understanding and identifying barriers to electric vehicle adoption through thematic analysis. *Transp. Res. Interdiscip. Perspect.* **2021**, *10*, 100364. [CrossRef]
7. Verma, A.; Singh, B.; Chandra, A.; Al-Haddad, K. An implementation of solar PV array based multifunctional EV charger. *IEEE Trans. Ind. Appl.* **2020**, *56*, 4166–4178. [CrossRef]
8. Ashique, R.H.; Salam, Z.; Aziz, M.J.B.A.; Bhatti, A.R. Integrated photovoltaic-grid dc fast charging system for electric vehicle: A review of the architecture and control. *Renew. Sustain. Energy Rev.* **2017**, *69*, 1243–1257. [CrossRef]
9. Youssef, C.; Fatima, E.; Chakib, A. A technological review on electric vehicle DC charging stations using photovoltaic sources. In *IOP Conference Series: Materials Science and Engineering*; IOP Publishing: Bristol, UK, 2018; Volume 1, p. 012014.
10. Şahin, A.D. Progress and recent trends in wind energy. *Prog. Energy Combust. Sci.* **2004**, *30*, 501–543. [CrossRef]
11. Huang, Q.; Jia, Q.S.; Guan, X. A review of EV load scheduling with wind power integration. *IFAC Pap.* **2015**, *48*, 223–228. [CrossRef]
12. Al Wahedi, A.; Bicer, Y. Development of an off-grid electrical vehicle charging station hybridized with renewables including battery cooling system and multiple energy storage units. *Energy Rep.* **2020**, *6*, 2006–2021. [CrossRef]
13. Vassilev, S.V.; Vassileva, C.G.; Vassilev, V.S. Advantages and disadvantages of composition and properties of biomass in comparison with coal: An overview. *Fuel* **2015**, *158*, 330–350. [CrossRef]
14. Blanco-Sanchez, P.; Taylor, D.; Cooper, S.; Hargreaves, N.; Bezanty, V.A. *IEA Bioenergy Task 33*; International Energy Agency: Paris, France, 2021.
15. Shemami, M.S.; Alam, M.S.; Asghar, M.S.J. Load shedding mitigation through plug-*in* electric vehicle-to-home (V2H) system. In Proceedings of the 2017 IEEE Transportation Electrification Conference and Expo (ITEC), Chicago, IL, USA, 22–24 June 2017; pp. 799–804.
16. Bouich, A.; Marí-Guaita, J.; Bouich, A.; Pradas, I.G.; Marí, B. Towards manufacture stable lead perovskite APbI3 (A= Cs, MA, FA) based solar cells with low-cost techniques. *Eng. Proc.* **2022**, *12*, 81.
17. Singh, A.K.; Mishra, A.K.; Gupta, K.K.; Bhatnagar, P.; Kim, T. An integrated converter with reduced components for electric vehicles utilizing solar and grid power sources. *IEEE Trans. Transp. Electrif.* **2020**, *6*, 439–452. [CrossRef]
18. Mouli, G.R.C.; Schijffelen, J.; van den Heuvel, M.; Kardolus, M.; Bauer, P. A 10 kW solar-powered bidirectional EV charger compatible with chademo and COMBO. *IEEE Trans. Power Electron.* **2018**, *34*, 1082–1098. [CrossRef]
19. Bhatti, A.R.; Salam, Z.; Aziz, M.J.B.A.; Yee, K.P. A critical review of electric vehicle charging using solar photovoltaic. *Int. J. Energy Res.* **2016**, *40*, 439–461. [CrossRef]
20. Bhatti, A.R.; Salam, Z.; Aziz, M.J.B.A.; Yee, K.P.; Ashique, R.H. Electric vehicles charging using photovoltaic: Status and technological review. *Renew. Sustain. Energy Rev.* **2016**, *54*, 34–47. [CrossRef]
21. CHAdeMO Association. *Technical Specifications of Quick Charger for the Electric Vehicle: CHAdeMO 1.0.1*; CHAdeMO Association: Tokyo, Japan, 2013.
22. *SAE Standard J1772_201710*; SAE Electric Vehicle and Plug-In Hybrid Electric Vehicle Conductive Charge Coupler. SAE International: Warrendale, PA, USA, 2010.
23. Wang, L.; Qin, Z.; Slangen, T.; Bauer, P.; Wijk, T.V. Grid Impact of Electric Vehicle Fast Charging Stations: Trends, Standards, Issues and Mitigation Measures—An Overview. *IEEE Open J. Power Electron.* **2021**, *2*, 56–74. [CrossRef]
24. Yilmaz, M.; Krein, P.T. Review of battery charger topologies, charging power levels, and infrastructure for plug-in electric and hybrid vehicles. *IEEE Trans. Power Electron.* **2012**, *28*, 2151–2169. [CrossRef]
25. Singh, A.K.; Badoni, M.; Tatte, Y.N. A multifunctional solar PV and grid based on-board converter for electric vehicles. *IEEE Trans. Veh. Technol.* **2020**, *69*, 3717–3727. [CrossRef]
26. Ul-Haq, A.; Cecati, C.; Al-Ammar, E.A. Modeling of a photovoltaic-powered electric vehicle charging station with vehicle-to-grid implementation. *Energies* **2016**, *10*, 4. [CrossRef]
27. Soeiro, T.B.; Maia, G.J.; Ortmann, M.S.; Heldwein, M.L. High efficiency three-phase unidirectional bucktype PFC rectifier concepts. In Proceedings of the IECON 2013-39th Annual Conference of the IEEE Industrial Electronics Society, Vienna, Austria, 10–13 November 2013; pp. 7763–7768.

28. Chae, B.; Kang, T.; Kang, T.; Suh, Y. Carrier based PWM for three-phase three-switch buck-type rectifier in EV rapid charging system. In Proceedings of the 2015 9th International Conference on Power Electronics and ECCE Asia (ICPE-ECCE Asia), Seoul, Korea, 1–5 June 2015; pp. 881–889.
29. Baumann, M.; Kolar, J.W. Parallel connection of two three-phase three-switch buck-type unity-power-factor rectifier systems with dc-link current balancing. *IEEE Trans. Ind. Electron.* **2007**, *54*, 3042–3053. [CrossRef]
30. Nussbaumer, T.; Kolar, J.W. Improving mains current quality for three-phase three-switch buck-type PWM rectifiers. *IEEE Trans. Power Electron.* **2006**, *21*, 967–973. [CrossRef]
31. Lei, J.; Feng, S.; Zhao, J.; Chen, W.; Wheeler, P.; Shi, M. An improved three-phase buck rectifier topology with reduced voltage stress on transistors. *IEEE Trans. Power Electron.* **2019**, *35*, 2458–2466. [CrossRef]
32. Chen, Q.; Xu, J.; Zeng, F.; Huang, R.; Wang, L. An Improved Three-Phase Buck Rectifier with Low Voltage Stress on Switching Devices. *IEEE Trans. Power Electron.* **2020**, *36*, 6168–6174. [CrossRef]
33. Chen, Q.; Xu, J.; Wang, L.; Huang, R.; Ma, H. Analysis and improvement of the effect of distributed parasitic capacitance on high-frequency high-density three-phase buck rectifier. *IEEE Trans. Power Electron.* **2020**, *36*, 6415–6428. [CrossRef]
34. Afsharian, J.; Xu, D.; Wu, B.; Gong, B.; Yang, Z. A new PWM and commutation scheme for one phase loss operation of three-phase isolated buck matrix-type rectifier. *IEEE Trans. Power Electron.* **2018**, *33*, 9854–9865. [CrossRef]
35. Greul, R.; Round, S.D.; Kolar, J.W. Analysis and Control of a Three-Phase, Unity Power Factor Y-Rectifier. *IEEE Trans. Power Electron.* **2007**, *22*, 1900–1911. [CrossRef]
36. Soeiro, T.B.; Kolar, J.W. Analysis of high-efficiency three-phase two-and three-level unidirectional hybrid rectifiers. *IEEE Trans. Ind. Electron.* **2012**, *60*, 3589–3601. [CrossRef]
37. Huber, L.; Kumar, M.; Jovanovic, M.M. Analysis, design, and evaluation of three-phase three-wire isolated ac-dc converter implemented with three single-phase converter modules. In Proceedings of the 2016 IEEE Applied Power Electronics Conference and Exposition (APEC), Long Beach, CA, USA, 20–24 March 2016; pp. 38–45.
38. Kolar, J.W.; Friedli, T. The essence of three-phase PFC rectifier systems. In Proceedings of the 2011 IEEE 33rd International Telecommunications Energy Conference (INTELEC), Amsterdam, The Netherlands, 9–13 October 2011; pp. 1–27.
39. Zhang, B.; Xie, S.; Wang, X.; Xu, J. Modulation method and control strategy for full-bridge-based swiss rectifier to achieve ZVS operation and suppress low-order harmonics of injected current. *IEEE Trans. Power Electron.* **2019**, *35*, 6512–6522. [CrossRef]
40. Friedli, T.; Hartmann, M.; Kolar, J.W. The essence of three-phase PFC rectifier systems—Part II. *IEEE Trans. Power Electron.* **2013**, *29*, 543–560. [CrossRef]
41. Schrittwieser, L.; Kolar, J.W.; Soeiro, T.B. Novel SWISS rectifier modulation scheme preventing input current distortions at sector boundaries. *IEEE Trans. Power Electron.* **2016**, *32*, 5771–5785. [CrossRef]
42. Halbig, J. 15kW Bidirectional Vienna PFC, 2014 IEEE Applied Power Electronics Conference and Exposition-APEC 2020 Presentations by STMicroelectronics, August 2020. Available online: https://www.st.com/content/dam/AME/2020/apec-2020/presentations/APEC2020_Vienna_Rectifier-virtual-FINAL.pdf (accessed on 21 June 2022).
43. Huber, L.; Kumar, M.; Jovanović, M.M. Performance comparison of three-step and six-step PWM in average-current-controlled three-phase six-switch boost PFC rectifier. In Proceedings of the 2015 IEEE Applied Power Electronics Conference and Exposition (APEC), Charlotte, NC, USA, 15–19 March 2015; pp. 1861–1868.
44. Mallik, A.; Ding, W.; Shi, C.; Khaligh, A. Input voltage sensorless duty compensation control for a three-phase boost PFC converter. *IEEE Trans. Ind. Appl.* **2016**, *53*, 1527–1537. [CrossRef]
45. Xu, D.; Feng, B.; Li, R.; Mino, K.; Umida, H. A zero voltage switching SVM (ZVS–SVM) controlled three-phase boost rectifier. *IEEE Trans. Power Electron.* **2007**, *22*, 978–986. [CrossRef]
46. Sha, D.; Xu, G.; Xu, Y. Utility direct interfaced charger/discharger employing unified voltage balance control for cascaded H-bridge units and decentralized control for CF-DAB modules. *IEEE Trans. Ind. Electron.* **2017**, *64*, 7831–7841. [CrossRef]
47. Zheng, Z.; Wang, K.; Xu, L.; Li, Y. A hybrid cascaded multilevel converter for battery energy management applied in electric vehicles. *IEEE Trans. Power Electron.* **2013**, *29*, 3537–3546. [CrossRef]
48. Qin, S.; Lei, Y.; Ye, Z.; Chou, D.; Pilawa-Podgurski, R.C. A high-power-density power factor correction front end based on seven-level flying capacitor multilevel converter. *IEEE J. Emerg. Sel. Top. Power Electron.* **2018**, *7*, 1883–1898. [CrossRef]
49. Chou, D.; Fernandez, K.; Pilawa-Podgurski, R.C. An interleaved 6-level GaN bidirectional converter for level II electric vehicle charging. In Proceedings of the 2019 IEEE Applied Power Electronics Conference and Exposition (APEC), Anaheim, CA, USA, 17–21 March 2019; pp. 594–600.
50. Kang, T.; Kim, C.; Suh, Y.; Park, H.; Kang, B.; Kim, D. A design and control of bi-directional non-isolated DC-DC converter for rapid electric vehicle charging system. In Proceedings of the 2012 Twenty-Seventh Annual IEEE Applied Power Electronics Conference and Exposition (APEC), Orlando, FL, USA, 5–9 February 2012; pp. 14–21.
51. Rivera, S.; Wu, B.; Kouro, S.; Yaramasu, V.; Wang, J. Electric vehicle charging station using a neutral point clamped converter with bipolar DC bus. *IEEE Trans. Ind. Electron.* **2014**, *62*, 1999–2009. [CrossRef]
52. Reis, F.E.U.; Torrico-Bascope, R.P.; Tofoli, F.L.; Bezerra, L.D.S. Bidirectional three-level stacked neutral-point-clamped converter for electric vehicle charging stations. *IEEE Access* **2020**, *8*, 37565–37577. [CrossRef]
53. Abarzadeh, M.; Khan, W.A.; Weise, N.; Al-Haddad, K.; EL-Refaie, A.M. A new configuration of paralleled modular anpc multilevel converter controlled by an improved modulation method for 1MHZ, 1MW EV charger. *IEEE Trans. Ind. Appl.* **2020**, *57*, 3164–3178. [CrossRef]

54. Rajendran, G.; Vaithilingam, C.A.; Misron, N.; Naidu, K.; Ahmed, M.R. Voltage Oriented Controller Based Vienna Rectifier for Electric Vehicle Charging Stations. *IEEE Access* **2021**, *9*, 50798–50809. [CrossRef]
55. Wang, H.; Dusmez, S.; Khaligh, A. Design and analysis of a full-bridge LLC-based PEV charger optimized for wide battery voltage range. *IEEE Trans. Veh. Technol.* **2013**, *63*, 1603–1613. [CrossRef]
56. Li, H.; Zhang, Z.; Wang, S.; Tang, J.; Ren, X.; Chen, Q. A 300-kHz 6.6-kW SiC bidirectional LLC onboard charger. *IEEE Trans. Ind. Electron.* **2019**, *67*, 1435–1445. [CrossRef]
57. Yan, Y.; Bai, H.; Foote, A.; Wang, W. Securing full-power-range zero-voltage switching in both steady-state and transient operations for a dual-active-bridge-based bidirectional electric vehicle charger. *IEEE Trans. Power Electron.* **2019**, *35*, 7506–7519. [CrossRef]
58. Assadi, S.A.; Matsumoto, H.; Moshirvaziri, M.; Nasr, M.; Zaman, M.S.; Trescases, O. Active saturation mitigation in high-density dual-active-bridge DC–DC converter for on-board EV charger applications. *IEEE Trans. Power Electron.* **2019**, *35*, 4376–4387. [CrossRef]
59. Xuan, Y.; Yang, X.; Chen, W.; Liu, T.; Hao, X. A three-level dual-active-bridge converter with blocking capacitors for bidirectional electric vehicle charger. *IEEE Access* **2019**, *7*, 173838–173847. [CrossRef]
60. Bezerra, P.A.; Krismer, F.; Burkart, R.M.; Kolar, J.W. Bidirectional isolated non-resonant dab dc-dc converter for ultra-wide input voltage range applications. In Proceedings of the 2014 International Power Electronics and Application Conference and Exposition, Shanghai, China, 5–8 November 2014; pp. 1038–1044.
61. Shi, K.; Zhang, D.; Zhou, Z.; Zhang, M.; Zhang, D.; Gu, Y. A novel phase-shift dual full-bridge converter with full soft-switching range and wide conversion range. *IEEE Trans. Power Electron.* **2015**, *31*, 7747–7760. [CrossRef]
62. Gill, L.; Ikari, T.; Kai, T.; Li, B.; Ngo, K.; Dong, D. Medium voltage dual active bridge using 3.3 kV SiC MOSFETs for EV charging application. In Proceedings of the 2019 IEEE Energy Conversion Congress and Exposition (ECCE), Baltimore, MD, USA, 29 September–3 October 2019; pp. 1237–1244.
63. Twiname, R.P.; Thrimawithana, D.J.; Madawala, U.K.; Baguley, C.A. A dual-active bridge topology with a tuned CLC network. *IEEE Trans. Power Electron.* **2014**, *30*, 6543–6550. [CrossRef]
64. Muthuraj, S.S.; Kanakesh, V.K.; Das, P.; Panda, S.K. Triple phase shift control of an LLL tank based bidirectional dual active bridge converter. *IEEE Trans. Power Electron.* **2016**, *32*, 8035–8053. [CrossRef]
65. Malan, W.L.; Vilathgamuwa, D.M.; Walker, G.R. Modeling and control of a resonant dual active bridge with a tuned CLLC network. *IEEE Trans. Power Electron.* **2015**, *31*, 7297–7310. [CrossRef]
66. He, P.; Khaligh, A. Comprehensive analyses and comparison of 1kW isolated DC–DC converters for bidirectional EV charging systems. *IEEE Trans. Transp. Electrif.* **2016**, *3*, 147–156. [CrossRef]
67. Xuan, Y.; Yang, X.; Chen, W.; Liu, T.; Hao, X. A novel three-level CLLC resonant DC–DC converter for bidirectional EV charger in DC microgrids. *IEEE Trans. Ind. Electron.* **2020**, *68*, 2334–2344. [CrossRef]
68. Yaqoob, M.; Loo, K.H.; Lai, Y.M. Extension of soft-switching region of dual-active-bridge converter by a tunable resonant tank. *IEEE Trans. Power Electron.* **2017**, *32*, 9093–9104. [CrossRef]
69. Corradini, L.; Seltzer, D.; Bloomquist, D.; Zane, R.; Maksimović, D.; Jacobson, B. Minimum current operation of bidirectional dual-bridge series resonant DC/DC converters. *IEEE Trans. Power Electron.* **2011**, *27*, 3266–3276. [CrossRef]
70. Li, X.; Bhat, A.K. Analysis and design of high-frequency isolated dual-bridge series resonant DC/DC converter. *IEEE Trans. Power Electron.* **2009**, *25*, 850–862.
71. Yaqoob, M.; Loo, K.H.; Lai, Y.M. A four-degrees-of-freedom modulation strategy for dual-active-bridge series-resonant converter designed for total loss minimization. *IEEE Trans. Power Electron.* **2018**, *34*, 1065–1081. [CrossRef]
72. Twiname, R.P.; Thrimawithana, D.J.; Madawala, U.K.; Baguley, C.A. A new resonant bidirectional DC–DC converter topology. *IEEE Trans. Power Electron.* **2013**, *29*, 4733–4740. [CrossRef]
73. Mishima, T.; Akamatsu, K.; Nakaoka, M. A high frequency-link secondary-side phase-shifted full-range soft-switching PWM DC–DC converter with ZCS active rectifier for EV battery chargers. *IEEE Trans. Power Electron.* **2013**, *28*, 5758–5773. [CrossRef]
74. Kanamarlapudi, V.R.K.; Wang, B.; Kandasamy, N.K.; So, P.L. A new ZVS full-bridge DC–DC converter for battery charging with reduced losses over full-load range. *IEEE Trans. Ind. Appl.* **2017**, *54*, 571–579. [CrossRef]
75. Lim, C.Y.; Jeong, Y.; Moon, G.W. Phase-shifted full-bridge DC–DC converter with high efficiency and high power density using center-tapped clamp circuit for battery charging in electric vehicles. *IEEE Trans. Power Electron.* **2019**, *34*, 10945–10959. [CrossRef]
76. Lim, C.Y.; Jeong, Y.; Lee, M.S.; Yi, K.H.; Moon, G.W. Half-bridge integrated phase-shifted full-bridge converter with high efficiency using center-tapped clamp circuit for battery charging systems in electric vehicles. *IEEE Trans. Power Electron.* **2019**, *35*, 4934–4945. [CrossRef]
77. Lee, I.O.; Cho, S.Y.; Moon, G.W. Interleaved buck converter having low switching losses and improved step-down conversion ratio. *IEEE Trans. Power Electron.* **2012**, *27*, 3664–3675. [CrossRef]
78. Drobnic, K.; Grandi, G.; Hammami, M.; Mandrioli, R.; Ricco, M.; Viatkin, A.; Vujacic, M. An output ripple-free fast charger for electric vehicles based on grid-tied modular three-phase interleaved converters. *IEEE Trans. Ind. Appl.* **2019**, *55*, 6102–6114. [CrossRef]
79. Hammami, M.; Viatkin, A.; Ricco, M.; Grandi, G. A dc/dc fast charger for electric vehicles with minimum input/output ripple based on multiphase interleaved converters. In Proceedings of the 2019 International Conference on Clean Electrical Power (ICCEP), Otranto, Italy, 2–4 July 2019; pp. 187–192.

80. Grbović, P.J.; Delarue, P.; Le Moigne, P.; Bartholomeus, P. A bidirectional three-level DC–DC converter for the ultracapacitor applications. *IEEE Trans. Ind. Electron.* **2009**, *57*, 3415–3430. [CrossRef]
81. Dusmez, S.; Hasanzadeh, A.; Khaligh, A. Comparative analysis of bidirectional three-level DC–DC converter for automotive applications. *IEEE Trans. Ind. Electron.* **2014**, *62*, 3305–3315. [CrossRef]
82. Monteiro, V.; Ferreira, J.C.; Melendez, A.A.N.; Couto, C.; Afonso, J.L. Experimental validation of a novel architecture based on a dual-stage converter for off-board fast battery chargers of electric vehicles. *IEEE Trans. Veh. Technol.* **2017**, *67*, 1000–1011. [CrossRef]
83. Monteiro, V.; Ferreira, J.C.; Melendez, A.A.N.; Afonso, J.A.; Couto, C.; Afonso, J.L. Experimental validation of a bidirectional three-level dc-dc converter for on-board or off-board EV battery chargers. In Proceedings of the IECON 2019-45th Annual Conference of the IEEE Industrial Electronics Society, Lisbon, Portugal, 14–17 October 2019; Volume 1, pp. 3468–3473.
84. Tan, L.; Wu, B.; Rivera, S.; Yaramasu, V. Comprehensive DC power balance management in high-power three-level DC–DC converter for electric vehicle fast charging. *IEEE Trans. Power Electron.* **2015**, *31*, 89–100. [CrossRef]
85. Tan, L.; Zhu, N.; Wu, B. An integrated inductor for eliminating circulating current of parallel three-level DC–DC converter-based EV fast charger. *IEEE Trans. Ind. Electron.* **2015**, *63*, 1362–1371. [CrossRef]
86. Monteiro, V.; Pinto, J.G.; Afonso, J.L. Experimental validation of a three-port integrated topology to interface electric vehicles and renewables with the electrical grid. *IEEE Trans. Ind. Inform.* **2018**, *14*, 2364–2374. [CrossRef]
87. Tazay, A.; Miao, Z. Control of a three-phase hybrid converter for a PV charging station. *IEEE Trans. Energy Convers.* **2018**, *33*, 1002–1014. [CrossRef]
88. Khan, S.A.; Islam, M.R.; Guo, Y.; Zhu, J. A new isolated multi-port converter with multi-directional power flow capabilities for smart electric vehicle charging stations. *IEEE Trans. Appl. Supercond.* **2019**, *29*, 1–4. [CrossRef]
89. Bhattacharjee, A.K.; Batarseh, I. An interleaved boost and dual active bridge-based single-stage three-port DC–DC–AC converter with sine PWM modulation. *IEEE Trans. Ind. Electron.* **2020**, *68*, 4790–4800. [CrossRef]
90. Murdock, H.E.; Gibb, D.; Andre, T.; Sawin, J.L.; Brown, A.; Ranalder Land Brumer, L. *Renewables 2021-Global Status Report*; UN Environment Programme: Paris, France, 2021.
91. Feldman, D.; Dummit, K.; Zuboy, J.; Heeter, J.; Xu, K.; Margolis, R. *Winter 2021/2022 Solar Industry Update (No. NREL/PR-7A40-81900)*; National Renewable Energy Lab. (NREL): Golden, CO, USA, 2022.
92. König, A.; Nicoletti, L.; Schröder, D.; Wolff, S.; Waclaw, A.; Lienkamp, M. An overview of parameter and cost for battery electric vehicles. *World Electr. Veh. J.* **2021**, *12*, 21. [CrossRef]
93. Khaligh, A.; D'Antonio, M. Global trends in high-power on-board chargers for electric vehicles. *IEEE Trans. Veh. Technol.* **2019**, *68*, 3306–3324. [CrossRef]
94. Plugs, S.-O. *Vehicle Connectors and Vehicle Inlets Conductive Charging of Electric Vehicles—Part 1, 2, 3*; IEC Standard 62196; IEC: Geneva, Switzerland, 2014; pp. 1–176.
95. Rivera, S.; Kouro, S.; Vazquez, S.; Goetz, S.M.; Lizana, R.; Romero-Cadaval, E. Electric vehicle charging infrastructure: From grid to battery. *IEEE Ind. Electron. Mag.* **2021**, *15*, 37–51. [CrossRef]
96. Liu, L.; Kong, F.; Liu, X.; Peng, Y.; Wang, Q. A review on electric vehicles interacting with renewable energy in smart grid. *Renew. Sustain. Energy Rev.* **2015**, *51*, 648–661. [CrossRef]
97. Tulpule, P.J.; Marano, V.; Yurkovich, S.; Rizzoni, G. Economic and environmental impacts of a PV powered workplace parking garage charging station. *Appl. Energy* **2013**, *108*, 323–332. [CrossRef]
98. Tong, S.J.; Same, A.; Kootstra, M.A.; Park, J.W. Off-grid photovoltaic vehicle charge using second life lithium batteries: An experimental and numerical investigation. *Appl. Energy* **2013**, *104*, 740–750. [CrossRef]
99. Mesentean, S.; Feucht, W.; Kula, H.G.; Frank, H. Smart charging of electric scooters for home to work and home to education transports from grid connected photovoltaic-systems. In Proceedings of the 2010 IEEE International Energy Conference, Manama, Bahrain, 18–22 December 2010; pp. 73–78.
100. Pantelimon, R.F.; Adam, M.; Andruşcă, M.; Pancu, C. Aspects regarding solar battery charge controllers. In Proceedings of the 2013 8th International Symposium on Advanced Topics in Electrical Engineering (ATEE), Bucharest, Romania, 23–25 May 2013; pp. 1–6.
101. Traube, J.; Lu, F.; Maksimovic, D. Electric vehicle DC charger integrated within a photovoltaic power system. In Proceedings of the 2012 Twenty-Seventh Annual IEEE Applied Power Electronics Conference and Exposition (APEC), Orlando, FL, USA, 5–9 February 2012; pp. 352–358.
102. Sbordone, D.; Bertini, I.; Di Pietra, B.; Falvo, M.C.; Genovese, A.; Martirano, L. EV fast charging stations and energy storage technologies: A real implementation in the smart micro grid paradigm. *Electr. Power Syst. Res.* **2015**, *120*, 96–108. [CrossRef]
103. Kurose, N.; Takahashi, R.; Tamura, J.; Fukushima, T.; Sasano, E.; Shinya, K. A consideration on the determination of power rating of energy storage system for smoothing wind generator output. In Proceedings of the 2010 International Conference on Electrical Machines and Systems, Incheon, Korea, 10–13 October 2010; pp. 622–627.
104. Niroomand, M.; Nasr Esfahani, F. Control Structures of Grid-Tied Photovoltaic Systems. In *Energy Conversion Systems: An Overview*; Tripathi, S.M., Padmanaban, S., Eds.; (Energy Science, Engineering and Technology); Nova Science Publishers: New York, NY, USA, 2021; pp. 59–133.
105. Brunton, S.L.; Rowley, C.W.; Kulkarni, S.R.; Clarkson, C. Maximum power point tracking for photovoltaic optimization using ripple-based extremum seeking control. *IEEE Trans. Power Electron.* **2010**, *25*, 2531–2540. [CrossRef]

106. Gavhane, P.S.; Krishnamurthy, S.; Dixit, R.; Ram, J.P.; Rajasekar, N. EL-PSO based MPPT for solar PV under partial shaded condition. *Energy Procedia* **2017**, *117*, 1047–1053. [CrossRef]
107. Chiu, C.S. TS fuzzy maximum power point tracking control of solar power generation systems. *IEEE Trans. Energy Convers.* **2010**, *25*, 1123–1132. [CrossRef]
108. Sahnoun, M.A.; Ugalde, H.M.R.; Carmona, J.C.; Gomand, J. Maximum power point tracking using PandO control optimized by a neural network approach: A good compromise between accuracy and complexity. *Energy Procedia* **2013**, *42*, 650–659. [CrossRef]
109. Li, S.; Liao, H.; Yuan, H.; Ai, Q.; Chen, K. A MPPT strategy with variable weather parameters through analyzing the effect of the DC/DC converter to the MPP of PV system. *Sol. Energy* **2017**, *144*, 175–184. [CrossRef]
110. Ahmed, J.; Salam, Z. An improved perturb and observe (PandO) maximum power point tracking (MPPT) algorithm for higher efficiency. *Appl. Energy* **2015**, *150*, 97–108. [CrossRef]
111. Sera, D.; Mathe, L.; Kerekes, T.; Spataru, S.V.; Teodorescu, R. On the perturb-and-observe and incremental conductance MPPT methods for PV systems. *IEEE J. Photovolt.* **2013**, *3*, 1070–1078. [CrossRef]
112. Niroomand, M.; Nasr Esfahani, F. Converter Technologies for PV Systems: A Comprehensive Review. In *Energy Conversion Systems: An Overview*; Tripathi, S.M., Padmanaban, S., Eds.; (Energy Science, Engineering and Technology); Nova Science Publishers: New York, NY, USA, 2021.
113. Uddin, K.; Moore, A.D.; Barai, A.; Marco, J. The effects of high frequency current ripple on electric vehicle battery performance. *Appl. Energy* **2016**, *178*, 142–154. [CrossRef]
114. Brand, M.J.; Hofmann, M.H.; Schuster, S.S.; Keil, P.; Jossen, A. The influence of current ripples on the lifetime of lithium-ion batteries. *IEEE Trans. Veh. Technol.* **2018**, *67*, 10438–10445. [CrossRef]
115. Garcia, O.; Zumel, P.; De Castro, A.; Cobos, A. Automotive DC-DC bidirectional converter made with many interleaved buck stages. *IEEE Trans. Power Electron.* **2006**, *21*, 578–586. [CrossRef]
116. Repecho, V.; Biel, D.; Ramos-Lara, R.; Vega, P.G. Fixed-switching frequency interleaved sliding mode eight-phase synchronous buck converter. *IEEE Trans. Power Electron.* **2017**, *33*, 676–688. [CrossRef]
117. Badawy, A.D. Current Source dc-dc and dc-ac Converters with Continuous Energy Flow. Ph.D. Thesis, University of Strathclyde, Glasgow, UK, 2015.
118. Patil, N.S.; Shukla, A. Review and Comparison of MV grid-connected Extreme Fast Charging Converters for Electric Vehicles. In Proceedings of the 2021 National Power Electronics Conference (NPEC), Bhubaneswar, India, 15–17 December 2021; pp. 1–6.
119. Haga, H.; Kurokawa, F. Modulation method of a full-bridge three-level LLC resonant converter for battery charger of electrical vehicles. *IEEE Trans. Power Electron.* **2016**, *32*, 2498–2507. [CrossRef]
120. Deng, J.; Li, S.; Hu, S.; Mi, C.C.; Ma, R. Design methodology of LLC resonant converters for electric vehicle battery chargers. *IEEE Trans. Veh. Technol.* **2013**, *63*, 1581–1592. [CrossRef]
121. Shahzad, M.I.; Iqbal, S.; Taib, S. Interleaved LLC converter with cascaded voltage-doubler rectifiers for deeply depleted PEV battery charging. *IEEE Trans. Transp. Electrif.* **2017**, *4*, 89–98. [CrossRef]
122. Dao, N.D.; Lee, D.C. High-efficiency hybrid LLC resonant converter for on-board chargers of plug-in electric vehicles. *IEEE Trans. Power Electron.* **2020**, *35*, 8324–8334.
123. Li, B.; Lee, F.C.; Li, Q.; Liu, Z. Bi-directional on-board charger architecture and control for achieving ultra-high efficiency with wide battery voltage range. In Proceedings of the 2017 IEEE Applied Power Electronics Conference and Exposition (APEC), Tampa, FL, USA, 26–30 March 2017; pp. 3688–3694.
124. Liu, C.; Wang, J.; Colombage, K.; Gould, C.; Sen, B. A CLLC resonant converter based bidirectional EV charger with maximum efficiency tracking. In Proceedings of the 8th IET International Conference on Power Electronics, Machines and Drives (PEMD 2016), Glasgow, UK, 19–21 April 2016; pp. 1–6.
125. Zahid, Z.U.; Dalala, Z.M.; Chen, R.; Chen, B.; Lai, J.S. Design of bidirectional DC–DC resonant converter for vehicle-to-grid (V2G) applications. *IEEE Trans. Transp. Electrif.* **2015**, *1*, 232–244. [CrossRef]
126. Kwon, M.; Oh, S.; Choi, S. High gain soft-switching bidirectional DC–DC converter for eco-friendly vehicles. *IEEE Trans. Power Electron.* **2013**, *29*, 1659–1666. [CrossRef]
127. Han, J.; Lim, C.S.; Cho, J.H.; Kim, R.Y.; Hyun, D.S. A high efficiency non-isolated bidirectional DC-DC converter with zero-voltage-transition. In Proceedings of the IECON 2013-39th Annual Conference of the IEEE Industrial Electronics Society, Vienna, Austria, 10–13 November 2013; pp. 198–203.
128. Rathore, A.K.; Prasanna, U.R. Analysis, design, and experimental results of novel snubberless bidirectional naturally clamped ZCS/ZVS current-fed half-bridge DC/DC converter for fuel cell vehicles. *IEEE Trans. Ind. Electron.* **2012**, *60*, 4482–4491. [CrossRef]
129. Zhang, J.; Lai, J.S.; Kim, R.Y.; Yu, W. High-power density design of a soft-switching high-power bidirectional DC–DC converter. *IEEE Trans. Power Electron.* **2007**, *22*, 1145–1153. [CrossRef]
130. Darwish, A.; Elgenedy, M.A.; Finney, S.J.; Williams, B.W.; McDonald, J.R. A step-up modular high-voltage pulse generator based on isolated input-parallel/output-series voltage-boosting modules and modular multilevel submodules. *IEEE Trans. Ind. Electron.* **2017**, *66*, 2207–2216. [CrossRef]
131. Darwish, A.; Elgenedy, M.A. Current-source modular medium-voltage grid-connected system with high-frequency isolation for photovoltaic applications. *IEEE Trans. Energy Convers.* **2018**, *34*, 255–266. [CrossRef]
132. Darwish, A.; Alotaibi, S.; Elgenedy, M.A. Current-source single-phase module integrated inverters for PV grid-connected applications. *IEEE Access* **2020**, *8*, 53082–53096. [CrossRef]

133. Maneiro, J.; Hassan, F. A flexible modular multi-level converter for DC microgrids with EV charging stations. In Proceedings of the 2013 Twenty-Eighth Annual IEEE Applied Power Electronics Conference and Exposition (APEC), Long Beach, CA, USA, 17–21 March 2013; pp. 1316–1320.
134. Ciccarelli, F.; Del Pizzo, A.; Iannuzzi, D. An ultra-fast charging architecture based on modular multilevel converters integrated with energy storage buffers. In Proceedings of the 2013 Eighth International Conference and Exhibition on Ecological Vehicles and Renewable Energies (EVER), Monte Carlo, Monaco, 27–30 March 2013; pp. 1–6.
135. Abronzini, U.; Attaianese, C.; D'Arpino, M.; Di Monaco, M.; Rufer, A.; Tomasso, G. Dead time and non-linearities compensation for CHB multi-level converters with integrated ESS feeding EV's ultra-fast charging stations. In Proceedings of the 2016 International Conference on Electrical Systems for Aircraft, Railway, Ship Propulsion and Road Vehicles and International Transportation Electrification Conference (ESARS-ITEC), Toulouse, France, 2–4 November 2016; pp. 1–5.
136. Abronzini, U.; Attaianese, C.; Di Monaco, M.; Tomasso, G.; D'Arpino, M. Optimal Control for CHB Multi-Level Converter with Integrated ESS for EV Ultra-Fast Charging Station. In Proceedings of the 2018 IEEE International Conference on Electrical Systems for Aircraft, Railway, Ship Propulsion and Road Vehicles and International Transportation Electrification Conference (ESARS-ITEC), Nottingham, UK, 7–9 November 2018; pp. 1–6.
137. Yan, Z.; Yin, Z.; Yang, X.; Zhang, K.; Shi, J.; Wang, L. Research and simulation of centralized charge and discharge technology of EVs based on MMC. In Proceedings of the 2017 2nd International Conference on Power and Renewable Energy (ICPRE), Chengdu, China, 20–23 September 2017; pp. 800–804.
138. Qashqai, P.; Sheikholeslami, A.; Vahedi, H.; Al-Haddad, K. A review on multilevel converter topologies for electric transportation applications. In Proceedings of the 2015 IEEE Vehicle Power and Propulsion Conference (VPPC), Montreal, QC, Canada, 19–22 October 2015; pp. 1–6.
139. Vadhiraj, S.; Swamy, K.N.; Divakar, B.P. Generic SPWM technique for multilevel inverter. In Proceedings of the 2013 IEEE PES Asia-Pacific Power and Energy Engineering Conference (APPEEC), Hong Kong, China, 8–11 December 2013; pp. 1–5.
140. McGrath, B.P.; Holmes, D.G.; Lipo, T. Optimized space vector switching sequences for multilevel inverters. *IEEE Trans. Power Electron.* **2003**, *18*, 1293–1301. [CrossRef]
141. Deng, Y.; Wang, Y.; Teo, K.H.; Harley, R.G. A simplified space vector modulation scheme for multilevel converters. *IEEE Trans. Power Electron.* **2015**, *31*, 1873–1886. [CrossRef]
142. Ronanki, D.; Williamson, S.S. Modular multilevel converters for transportation electrification: Challenges and opportunities. *IEEE Trans. Transp. Electrif.* **2018**, *4*, 399–407. [CrossRef]
143. Alotaibi, S.; Darwish, A. Modular Multilevel Converters for Large-Scale Grid-Connected Photovoltaic Systems: A Review. *Energies* **2021**, *14*, 6213. [CrossRef]